UNIVERSIDAD NACIONAL AUTÓNOMA DE MÉXICO
DOCTORADO EN CIENCIAS BIOMÉDICAS
INSTITUTO DE FISIOLOGÍA CELULAR
DEPARTAMENTO DE NEUROCIENCIAS COGNITIVAS

ACCIONES DE NEURONAS PV+ EN LOS ENSAMBLES NEURONALES

T E S I S

QUE PARA OPTAR POR EL GRADO DE:
DOCTORA EN CIENCIAS

PRESENTA:
MARIANA DUHNE RAMÍREZ

TUTOR PRINCIPAL:
DR. JOSÉ BARGAS DÍAZ
INSTITUTO DE FISIOLOGÍA CELULAR

COMITÉ TUTOR:
DRA. ALICIA GONZÁLEZ
INSTITUTO DE FISIOLOGÍA CELULAR
DR. JOSÉ FERNANDO PEÑA ORTEGA
INSTITUTO DE NEUROBIOLOGÍA

CIUDAD UNIVERSITARIA, CD. MX., FEBRERO 2020

Agradecimientos académicos

Al Dr. José Bargas Díaz por todo el apoyo en el desarrollo de este y otros proyectos y por su apoyo en mi formación académica.

Al Físico Juan Antonio Laville Conde por todo su apoyo en el desarrollo del proyecto y la solución de problemas técnicos.

Al Biol. Dagoberto Tapia Ramirez por todo su apoyo en el laboratorio.

A la M.V.Z. Claudia V. Rivera, al M.V.Z. Héctor Malagón Rivero, la M.C. Gabriela Xóchitl Ayala Méndez y la Dra. Ariadna Aparicio Juárez por el apoyo en el cuidado y manejo de animales.

A la Dra. Yazmín Ramiro Cortés y la Unidad de Imagenología del IFC por su apoyo.

A la unidad de cómputo del IFC, Ana María Escalante Gonzalbo y a Francisco Pérez Eugenio.

A los ingenieros del Taller de Mantenimiento del IFC, UNAM: el Ing. Aurey Galván Lobato y el Ing. Manuel Ortínez Benavides por su apoyo y asesoría en el mantenimiento y operación de los equipos de Investigación del Laboratorio.

Al Posgrado en Ciencias Biomédicas de la Universidad Nacional Autónoma de México.

Al Instituto de Fisiología Celular

Al CONACyT por la beca 270245 otorgada

Índice

Resumen

El estriado es el principal núcleo de entrada de los ganglios basales. Su actividad está dada por microcircuitos que se manifiestan como la activación secuencial de grupos de neuronas que forman una red dinámica. Estos se activan en condiciones control al presentarse un estímulo excitador, por ejemplo, un estímulo cortical, o la adición de bajas concentraciones de NMDA u otros fármacos al tejido cerebral. En condiciones patológicas, tales como los modelos animales de la enfermedad de Parkinson, la actividad de los circuitos aumenta espontáneamente, en estas condiciones un grupo dominante, altamente recurrente, impide la generación de secuencias de actividad. Hasta el momento se desconoce cómo participan los distintos tipos neuronales dentro de los grupos y cómo modulan la aparición de sus secuencias temporales. La alternancia entre distintos grupos para formar secuencias requiere de interconectividad entre ellos, probablemente dada por interneuronas que son el blanco preferente de las aferentes al estriado. Una clase importante de interneuronas expresa la proteína parvalbúmina (PV+); se le atribuye la mediación de la inhibición *feedforward*. Sin embargo, se desconoce qué otras acciones realizan estas interneuronas en el microcircuito. Utilizando imagenología de calcio in vitro en rebanadas de ratones transgénicos PV Cre, registramos la actividad de docenas de neuronas simultáneamente al mismo tiempo que identificamos a las interneuronas PV+. En este contexto, aunque anatómicamente sólo son el 1% de las neuronas del núcleo, resultaron ser el 5-11% de las neuronas que disparan cuando se activa un microcircuito. Al activar a estas interneuronas con optogenética en un circuito sin estimular o en reposo, sucede que se activan más neuronas de las que son inhibidas, lo cual demuestra que la inhibición no es su única función. En un microcircuito estimulado o activo la

activación de las interneuronas PV+ produce una reconfiguración de los ensambles neuronales presentes cambiando las conexiones funcionales entre ellas y su pertenencia a determinados ensambles. Este puede ser un mecanismo que explique la alternancia entre la activación de los ensambles, provocando distintas secuencias de activación.

Abstract

The striatum is the largest entrance nucleus to the basal ganglia. It presents microcircuit activity, consisting in the sequential activation of neuronal ensembles, groups of neurons that activate together. How different neuron classes present in the striatum participate in generating ensembles sequences is unknown. Microcircuit activity can be studied by recording the activity of brain slices *in vitro* with calcium imaging. Providing excitatory drive to the striatum generates ensembles sequences. In Parkinsonian microcircuits the activity is captured by a highly recurrent ensemble, which suppresses the appearance of ensemble sequences, cortical stimulus causes a transitory reconfiguration of neuronal groups alleviating Parkinsonism. Alternation between neuronal ensembles needs interconnectivity, in part due to interneurons, preferentially innervated by incoming afferents. One main class of interneuron expresses parvalbumin (PV+ neurons) and mediates feedforward inhibition. However, its more global actions within the microcircuit are unknown. Using calcium imaging *ex vivo* in brain slices simultaneously recording dozens of neurons we aimed to observe the actions of PV+ neurons within the striatal microcircuit. PV+ neurons in active microcircuits are 5-11% of the active neurons even if, anatomically, they are less than 1% of the total neuronal population. In resting microcircuits, optogenetic activation of PV+ neurons ignites circuit activity by activating or disinhibiting, more neurons than those actually inhibited, showing that feedforward inhibition is not their only function. Optostimulation of PV+ neurons in active microcircuits inhibits and activates different neuron sets, resulting in reconfiguration of neuronal ensembles by changing their functional connections and ensemble membership, showing that neurons may belong to

different ensembles at different situations. Our results demonstrate that PV+ neurons participate in the mechanisms that generate alternation of neuronal ensembles therefore provoking ensemble sequences.

Introducción

Microcircuito estriatal

El estriado (NSt o caudado putamen) es el principal núcleo de entrada de los ganglios basales, sus funciones incluyen el control de movimientos, la memoria de procedimientos y el control automático de la postura y el tono muscular para preservar el centro de masa (Graybiel, 1995b). Desbalances en la función estriatal se asocian con diversos problemas como la enfermedad de Parkinson y Huntington (Turner & Desmurget, 2010). Trabajo previo ha demostrado la presencia de una dinámica de microcircuitos en el NSt consistente en la activación secuencial de ensambles neuronales que codifican comportamiento y neuromodulación (Carrillo-Reid *et al.*, 2009; Jin *et al.*, 2014; Pérez-Ortega *et al.*, 2016; Sheng *et al.*, 2019).

Un microcircuito neuronal se define como la configuración funcional utilizada por las células nerviosas para llevar a cabo operaciones específicas. De esta organización dependen diferentes funciones cognitivas o las automáticas, algunas presentes desde el nacimiento tales como la succión, deglución, locomoción, prensión, etc. (Selverston, 1999). Los circuitos innatos encargados de los programas motores automáticos se denominan “Generadores Centrales de Pautas”, entendiéndose por “pauta” una actividad temporalmente estereotipada encaminada a un fin (CPGs por sus siglas en inglés, *Central Pattern Generators*), descritos inicialmente por Brown (1911) y presentes en la mayor parte de los vertebrados. A pesar de ser innatos, estos circuitos pueden aprender y adaptarse gracias a la plasticidad sináptica (Feldman *et al.*, 2003).

Los circuitos que llevan a cabo las funciones cognitivas se supone que no son innatos sino adquiridos, los postuló Hebb (1949) de manera hipotética y muy recientemente se ha recopilado evidencia de que existen, tanto por electrofisiología como por imagenología, se les ha denominado "Ensambles Celulares" (Cas por sus siglas en inglés, *Cell Assemblies*) (Carrillo-Reid *et al.*, 2008; Buzsaki, 2010).

Se supone que el estriado posee ambos tipos de circuitos: los CPGs encargados de ajustes automáticos de la postura y los CAs encargados de guardar memorias de procedimientos y hábitos (Barnes *et al.*, 2005; Carrillo-Reid *et al.*, 2008; Graybiel, 1995a).

Las características más importantes de ambos microcircuitos son: 1) presentan una salida estructurada temporalmente, a pesar de que las entradas no estén estructuradas (Grillner & El Manira, 2015). 2) Su operación se mantiene *in vitro* siempre y cuando se mantenga una estimulación mínima tal como adición de NMDA en la perfusión (Grillner & El Manira, 2015), una entrada tónica aferente (*excitatory tonic drive*), etc. 3) Su operación se manifiesta por presentar "ciclos de actividad" que comienzan y terminan en el mismo grupo de neuronas (reverberantes), por lo que se piensa son la base de la memoria de trabajo (Barnes *et al.*, 2005), 4) Exigen un determinado grado de sincronización o disparo correlacionado de las neuronas participantes, esto es, el flujo de actividad que viaja por el tejido es el disparo sincrónico de grupos de neuronas que se alternan la actividad, 5) Esta actividad se manifiesta por biestabilidad en las neuronas, esto es, por despolarizaciones espontáneas que sostienen disparo en ráfagas (*bursts*) de manera recurrente, por último, 6) Se supone que todo esto depende de trayectorias definidas o preferentes en la red neural ya sea por ser innatas o bien por haberse creado gracias a la plasticidad de largo plazo.

La presencia de CPGs y CAs en el NSt se ha demostrado previamente en el laboratorio, ya que hay disparo en ráfagas recurrentes en respuesta a un estímulo no correlacionado, como es la adición de NMDA en el medio (Vergara *et al.*, 2003). La actividad estimulada *in vitro* se corresponde *in vivo* a una conducta tal como la conducta de giro inducida por una inyección unilateral de NMDA (Ossowska & Wolfarth, 1995). La actividad en ráfagas recurrentes ocurre de manera sincrónica o correlacionada en varias neuronas ("vectores neurales"; Carrillo-Reid *et al.*, 2008), que alternan la actividad con otros varios grupos neuronales generando ciclos de actividad reverberante (Carrillo-Reid et al. 2008; 2009).

De manera adicional, en el laboratorio se ha estudiado el cambio en esta dinámica, en rebanadas cerebrales *ex vivo* de animales control. En estas condiciones el tejido sin estimulación o "en reposo", tiene poca actividad espontánea. Contrariamente, microcircuitos privados de dopamina sin estimulación, exhiben una alta actividad espontánea monopolizada por un ensamble neuronal o estado de la red dominante y altamente recurrente (Jáidar *et al.*, 2010; 2019; Pérez-Ortega *et al.*, 2016). Además de la adición de bajas concentraciones de NMDA como en el caso de los CPGs, la estimulación cortico-estriatal *in vitro* genera secuencias temporales de ensambles que alternan la actividad y que se mantienen por varios minutos, a este estado de la red le llamamos microcircuito estimulado o activo. Es interesante que la estimulación cortical en un circuito parkinsoniano o reducido en dopamina es capaz de disolver temporalmente el estado dominante, regresando a situaciones control de manera temporal (Aparicio-Juárez *et al.*, 2019; Lara-González *et al.*, 2019).

Poblaciones Neuronales del NSt

Cerca del 90% de las neuronas del estriado corresponden a neuronas espinosas de proyección (SPNs por sus siglas en inglés, spiny projection neurons) (Gerfen & Surmeier 2011; Graveland & DiFiglia 1985). Estas se categorizan en dos grandes grupos, las de la vía directa (dSPNs por sus siglas en inglés, direct pathway spiny projection neurons), que proyectan directamente a los núcleos de salida de los ganglios basales que son la sustancia nigra pars reticulata y el segmento interno del globo pálido y expresan receptor a dopamina de la clase D1, y las neuronas de la vía indirecta (iSPNs por sus siglas en inglés, indirect pathway spiny projection neurons), que proyectan exclusivamente al segmento externo del globo pálido, expresan receptor a dopamina de la clase D2. Desde el globo pálido externo, estas neuronas conectan con diversas vías de relevo, entre ellas la que la que toma de blanco al subtálamo y de ahí a los núcleos de salida llamada vía indirecta. Ambos tipos de neuronas pueden pertenecer a los mismos ensambles durante la ejecución de tareas motoras aprendidas, ya que se ha demostrado que ambos tipos de neurona reciben aferencia cortical y talámica similar (Doig *et al.*, 2010), ambas se activan para la ejecución de tareas motoras e iniciación de movimientos (Tecuapetla *et al.*, 2014; 2016) con una organización espaciotemporal específica (Klaus *et al.,* 2017), las neuronas pueden participar en diferentes ensambles neuronales que codifican para diferentes tareas o acciones (Sheng *et al.*, 2019).

El 10% restante de la población estriatal corresponde a diferentes tipos de interneuronas (Kawaguchi *et al.*, 1995). La mayoría de estas son GABAérgicas, aunque hay una pequeña porción de interneuronas que liberan acetilcolina por lo que expresan

colinacetiltransferasa (ChAT, por sus siglas en inglés) y electrofisiológicamente presentan disparo tónico a baja frecuencia. Las interneuronas GABAérgicas pueden clasificarse de acuerdo con su fenotipo electrofisiológico en: neuronas de disparo rápido o *fast-spiking interneurons* (FSI) que expresan la proteína parvalbumina (PV), neuronas de disparo de bajo umbral o *low-threshold spiking* (LTS) que se identifican por la expresión de somatostatina, algunas de estas neuronas presentan mesetas con potenciales prolongados (PLTS). Las neuronas que expresan somatostatina también pueden expresar neuropéptido Y (NPY) y óxido nítrico sintasa (NOS) (Tepper & Bolam 2004; Tepper *et al.*, 2010; Tepper & Kóos, 2017). También se han descrito marcadores neuronales que no corresponden a un único tipo neuronal, la enzima tirosina hidroxilasa (TH) se utiliza para marcar otra población de interneuronas que corresponde a diferentes fenotipos, el más común es el de las neuronas neurogliformes (NGF) (Ibáñez-Sandoval *et al.*, 2010). Otro subtipo expresa calretinina y del cual se sabe poco. Por último, se ha descrito una población que expresa el receptor a serotonina del tipo 5Ht3a. Este marcador puede colocalizar con PV, NPY, TH y CR. Estas interneuronas neuronas presentan al menos tres fenotipos electrofisiológicos distintos (Muñoz-Manchado *et al.*, 2016).

Tanto las SPNs como las diferentes poblaciones de interneuronas reciben aferencias corticales y talámicas (Arias-García *et al.*, 2018; Assous & Tepper, 2019). Se ha descrito que las interneuronas reciben entradas excitatorias de manera preferente y esto les permite ejercer control sobre poblaciones de SPNs (Koós & Tepper, 2004). Por lo que la señal de salida de las SPNs se encuentra ampliamente modulada por las interneuronas y la inhibición lateral entre ellas (Burke *et al.*, 2017). En particular, el papel que ejercen las FSI generando inhibición ante la

llegada de comandos motores denominada *feedforward* ha sido ampliamente estudiado (Gittis *et al.*, 2010; Mallet *et al.*, 2005).

Interneuronas de disparo rápido

Las interneuronas de disparo rápido o FSI se identifican por la expresión de parvalbúmina (PV). Son menos del 1% de las neuronas estriatales (Luk & Sadikot, 2001). Reciben una gran cantidad de entradas talámicas y corticales, incluso hay una mayor convergencia de estas proyecciones hacia esta población que hacia las SPNs (Choi *et al.*, 2019), dichas conexiones provienen de diferentes áreas corticales denotando un papel importante para la integración sensoriomotora (Lee *et al.*, 2019; Ramanathan *et al.*, 2002). Las FSI son más responsivas a pulsos corticales que las SPNs (Mallet *et al.*, 2005) y tienen mayor expresión de cFos en respuesta a estimulación cortical que las SPNs (Parthasarathy & Graybiel, 1997). Cada SPN recibe entradas sinápticas de 2-4 FSIs (Rymar *et al.*, 2004; Tepper & Koós, 2017) dado el gran árbol axónico que poseen. Cada FS tiene comunicación sináptica mediada por receptores $GABA_A$ al soma de decenas o cientos de SPNs (Tepper & Bolam, 2004; Straub *et al.*, 2016). Generan corrientes posinápticas inhibitorias de mayor amplitud en comparación con las SPNs sobre otras SPNs (Koós *et al.*, 2004; Tecuapetla *et al.*, 2007). Las FSIs también presentan una alta conectividad entre ellas por conexiones sinápticas y uniones comunicantes (Gittis *et al.*, 2010; Kita *et al.*, 1990; Russo *et al.*, 2013; Tepper & Koós, 2017), lo que podría dar lugar a un mecanismo de coordinación entre ellas.

Electrofisiológicamente se pueden identificar en registros extracelulares porque tienen potenciales de acción muy cortos (Kawaguchi, 1993) y disparan a frecuencias más altas que las

SPNs (Kawaguchi, 1995) sin adaptación en su frecuencia de disparo. En respuesta a entradas sinápticas disparan en ráfagas breves de potenciales de acción generalmente en el rango de la frecuencia gamma (Beatty *et al.*, 2015; Higgs & Wilson, 2019). Se cree que esta propiedad es especialmente importante para organizar a las neuronas de proyección en ensambles neuronales como mecanismo de selección e inhibición de estas (Buzsaki, 2010). El disparo de las FSI puede fácilmente inhibir el disparo de potenciales de acción de las SPNs (Koós & Tepper, 1999; Planert *et al.*, 2010). Permitiendo desinhibir o activar ensambles adyacentes (Lee *et al.,* 2018; Roberts *et al.*, 2019). Por ello se dice que sus funciones más importantes son la de generar inhibición *feedforward* y filtrar los comandos motores provenientes de la corteza.

Aunado a las propiedades descritas se ha demostrado su importancia funcional *in vivo,* la ablación de esta población produce cambios conductuales como exceso de acicalamiento (Xu *et al.*, 2016). Manipulaciones puntuales como la inhibición farmacológica específica de las FSI genera disquinesias (Gittis *et al.*, 2011). La manipulación optogenética de esta población puede mejorar la ejecución de tareas de discriminación (Lee *et al.*, 2018). Finalmente, se ha demostrado que son importantes para el aprendizaje de tareas y la ejecución de tareas egocéntricas (Owen *et al.*, 2018). Sin embargo, al registrar la actividad de FSI no se encuentra correlación significativa entre ellas ni parece ser modulada por eventos conductuales específicos como la recompensa, por lo que se cree pueden tener un rol más complejo en el procesamiento de información (Berke, 2008). Es necesario estudiar de manera más específica esta población de interneuronas y su interacción con docenas de neuronas adyacentes para elucidar su posible papel en la configuración de secuencias de ensambles, su patrón de conectividad y capacidad de generar sincronización y alternancia.

Planteamiento del Problema

Las neuronas PV+ son menos del 1% de las neuronas estriatales (Luk & Sadikot, 2001). Sin embargo, reciben mayor aferencia cortical (Choi *et al.*, 2019) la cual es importante para la integración sensorimotora (Lee *et al.*, 2019). Estudios de registro de pares han descrito que estas neuronas generan corrientes postsinápticas inhibitorias de gran amplitud sobre SPNs (Tecuapetla *et al.*, 2007) lo cuál se cree es un mecanismo para la generación de inhibición *feedforward* (Gittis *et al.*, 2010). Esta inhibición se ha relacionado con la supresión de acciones no deseadas *in vivo* (Xu *et al.*, 2016). Esta evidencia sugiere que la función que tienen este grupo de neuronas es de gran importancia a pesar de ser una pequeña porción de la población neuronal estriatal total. Hasta este momento se desconoce la participación de estas neuronas en la actividad del microcircuitos estriatales así como la función que desempeñan en la configuración de la dinámica del microcircuito. Y el efecto que pueden tener sobre la actividad de neuronas adjacentes.

Objetivos

- Describir la participación que tienen las neuronas PV+ en el microcircuito estriatal activo o estimulado.
- Analizar el efecto de activar a las neuronas PV+ en un microcircuito estriatal en reposo o sin estimulación.
- Analizar el efecto de activar a las neuronas PV+ en un microcircuito estriatal activado.

Hipótesis

Debido a su importancia funcional, la participación de las neuronas PV+ en un microcircuito activo debe ser mayor al 1% que es su proporción dada por análisis histológicos, reportados en la literatura. Estimular a las neuronas PV+ en un circuito silente generará un cambio de estado en la red. Al activar a las neuronas PV+ en un microcircuito activado se inhibirá la actividad de este y se reconfigurará la dinámica del microcircuito.

Material y Métodos

Sujetos experimentales

Todos los experimentos fueron realizados con ratones transgénicos PV-Cre obtenidos de Jackson Laboratories B6;129P2-Pvalbtm1(cre)Arbr/J (JAX stock:017320, Hippenmeyer *et al.*, 2005). La línea de animales se mantuvo en las instalaciones del bioterio del IFC y la cruza de estos se realizó entre homocigotos. Posterior a las cirugías los animales se mantuvieron en el vivario del IFC. Ambas instalaciones cuentan con temperatura controlada, ciclo luz: obscuridad de 12:12 h, con agua y comida estándar *ad libitum*.

Cirugía estereotáxica

Para la cirugía se usaron ratones de 30-35 días de edad, se anestesiaron por vía intraperitoneal con una solución de ketamina (85 mg/kg)-xilacina (15 mg/kg). Posteriormente, se colocó al animal en un aparato estereotáxico para ratón, se rasuró la parte superior del cráneo y se realizó una inyección subcutánea de lidocaína. Se hizo una incisión en la piel con bisturí y se inyectaron 0.5 µL de virus (dilución 1:1 para coexpresión) en las coordenadas +0.8 mm anteroposterior, -1.7 mm latero-medial y -3.0 mm dorsoventral desde Bregma, a una velocidad de 0.1 µL/min con una aguja dental (30 G). La aguja se dejó en el sitio de inyección por 10 min para permitir la difusión del virus. Posteriormente se sacó la aguja y se suturó la piel. La temperatura se controló durante la cirugía y hasta que el animal se recuperó de la anestesia. En los ojos se colocaron lágrimas artificiales para evitar daño a la córnea. Para realizar los experimentos se esperó un periodo de 10-21 días posteriores a la operación en la

cual los cuidados posoperatorios incluían una dieta con las suficientes calorías para mantener el peso de los ratones control.

Virus Adeno-asociados

Para la expresión de proteínas exógenas se utilizó la infección con los siguientes virus adeno-asociados a una concentración ≥ 7×10^{12} vg/mL, adquiridos de la compañía Addgene: para la expresión del canal de rodopsina 2 (*channelrhodopsin-2*, ChR2) se usó el virus pAAV-EF1a-double floxed-hChR2(H134R)-EYFP-WPRE-HGHpA donado por Karl Deisseroth (Addgene viral prep # 20298-AAV1; http://n2t.net/addgene:20298; RRID:Addgene_20298); para la expresión del indicador de calcio genéticamente codificado rojo (Red Genetically Encoded Calcium indicator for optical imaging, jRGECO) se usó pAAV.Syn.NES-jRGECO1b.WPRE.SV40, para la expresión del indicador de calcio genéticamente codificado verde (GCaMP6f) se usó pAAV.Syn.Flex.GCaMP6f.WPRE.SV40 y pAAV.Syn.GCaMP6f.WPRE.SV40 (jRGECO y GCaMP6f) ambos fueron donados por The Genetically Encoded Neuronal Indicator and Effector Project (GENIE) y Douglas Kim (Addgene viral prep # 100857-AAV1; http://n2t.net/addgene:100857; RRID:Addgene_100857; Addgene viral prep # 100837-AAV1; http://n2t.net/addgene:100837 ; RRID:Addgene_100837; Addgene viral prep # 100833-AAV1; http://n2t.net/addgene:100833 ; RRID:Addgene_100833, Dana *et al.,* 2016); para la expresión de la proteína fluorescente roja tdTomato, AAV pCAG-FLEX-tdTomato-WPRE; para la expresión de la proteína verde fluorescente (Enhanced Green Fluorescent Protein, EGFP), AAV pCAG-FLEX-EGFP-WPRE, ambos (tdTomato y EGFP) donados por Hongkui Zeng (Addgene viral prep # 51503-AAV1;

http://n2t.net/addgene:51503; RRID: Addgene_51503; Addgene viral prep # 5102-AAV1 ; http://n2t.net/addgene:51502 ; RRID:Addgene_51502, Oh *et al.,* 2014).

Inmunohistoquímica

Para comprobar la selectividad de la infección con virus se realizaron tinciones inmunohistoquímicas. Para ello, las rebanadas utilizadas para registro se incubaron 16-20 h en solución fijadora (buffer de fosfatos, PBS 0.1 M, paraformaldehído, PFA 4%, ácido pícrico 1%, pH=7.4). Para bloquear se incubaron con albúmina de suero bovino (BSA) 1% en PBS 0.1M (pH7.2) por 30 min. Se realizaron 3 lavados de 10 min con PBS posteriormente se incubaron con el anticuerpo primario anti-PV (Abcam Cat# ab11427, RRID: AB_298032) 1:1000 en PBS, tritón 2.5%, a 4°C por 24 h. Después se realizaron 3 lavados de 10 min con PBS. Se incubaron con el anticuerpo secundario anti-rabbit Alexa Fluor 647 (Jackson ImmunoResearch Labs Cat# 711-605-152, RRID: AB_2492288) 1:500 en PBS/tritón por 1.5 h y se hicieron 3 lavados de 10 min con PBS. Finalmente se montaron en laminillas selladas con medio de montaje para fluorescencia (Vecta Shield, Vector Laboratories, Inc. H-1200).

Microscopía confocal

Las imágenes de microscopía confocal se adquirieron con un microscopio Zeiss LSM-710 (objetivo: C-Apochromat 20X N.A. 0.45). Para los diferentes fluoróforos se utilizaron los siguientes parámetros de adquisición: GCamp6f, 488 nm laser excitación (ex), 493-533 nm emisión (em); tdTomato, 543 nm laser ex., 565-615 nm em.; Alexa 647, 633 nm laser ex., 658-704 nm em.; eYFP, 514 nm laser ex., 519-565 nm em.; RGECO, 543 nm laser ex., 586-630 em).

Obtención de rebanadas cerebrales

Los animales se anestesiaron con ketamina/xilacina (85/15 mg/kg) intraperitoneal y se perfundieron con una solución de sacarosa (sacarosa 234 mM, $NaHCO_3$ 28mM, dextrosa 7 mM, piruvato 4.54 mM, ácido ascórbico 0.28 mM, KCl 2.5 mM, $MgCl_2$ 7mM, NaH_2PO_4 1.44 mM y $CaCl_2$ 0.4 mM) a 4°C saturadas con carbógeno (95% O_2, 5% CO_2). Posteriormente el ratón fue decapitado y se extrajo el cerebro del cual se obtuvieron rebanadas horizontales con un ángulo de 30° de 250 µm de grosor con un vibratomo (PELCO easiSlicer), con la misma solución de sacarosa. A partir de este momento las rebanadas se mantuvieron en fluido cerebroespinal artificial (NaCl 126 mM, dextrosa 10 mM, $NaHCO_3$ 26 mM, tiourea 0.2 mM, ácido ascórbico 0.2 mM, KCl 2.5 mM, $MgCl_2$ 1.3 mM, NaH_2PO_4 1.2 mM, $CaCl_2$ 2 mM), referido a partir de ahora como ACSF (por sus siglas en inglés), saturado de oxígeno por burbujeo con carbógeno.

Registros de Imagenología de Calcio

Las rebanadas se fijaron en una cámara de registro con perfusión constante de ACSF bajo un objetivo de inmersión 20X, 0.95 N.A. (XLUMPlanFI, Olympus). El tamaño de campo observado fue de 800 x 800 µm. La estimulación de los fluoróforos se realizó con una lámpara LED (Lambda HPX High Power LED driver). Para los diferentes fluoróforos se utilizaron los siguientes filtros: GCamp6f: excitación BP460-480 nm, emisión 495-540 nm (Olympus, U-MGFPHQ). tdTomato: excitación 565/20 nm (Chroma Technology Corporation, D565/20m), emisión 610/75 nm (Chroma Technology Corporation, HQ610/75m). RGECO: excitación 570/17nm (Chroma Technology Corporation, ETS570/17m) emisión 590 LP (Chroma Technology Corporation, ET590lp). Se adquirieron videos de 2160 cuadros obtenidos con una frecuencia de

6 cuadros por segundo con una cámara CoolSnap K4, controlada por el software Im-Patch© (www.impatch.ifc.unam.mx). Para observar la actividad de neuronas PV+ se usó la expresión de tdTomato-GCaMP6f, las rebanadas fueron estimuladas con un tren de 10 pulsos a 40 Hz con un electrodo bipolar concéntrico (FHC, #CBCFE75, 1.1-1.3 mA). Para la estimulación de neuronas PV+ se usó la coexpresión de ChR2-RGECO. La estimulación de luz fue de 5 estímulos de 10 pulsos a 40 Hz usando un láser de 473 nm de longitud de onda (CrystaLaser® 473 nm) acoplado a una fibra óptica de 200 nm colocada junto a la rebanada la intensidad de luz medida al final de la fibra óptica fue de 5-10 mW. Se utilizó un estímulo de 40 Hz ya que se ha demostrado mayor resonancia de las interneuronas PV+ en frecuencias cercanas a ésta (Beatty *et al.*, 2015). Al final de cada experimento se aplicó una solución con KCl 15 mM para evaluar la viabilidad de la rebanada, solo se analizaron aquellos experimentos en que al menos el 85% de las células cargadas con fluoróforo estuvieran viables.

Registros electrofisiológicos

Para comprobar la identidad de las neuronas PV+ y comprobar la especificidad de la estimulación optogenética se realizaron registros electrofisiológicos de neuronas PV+ identificadas. Además, se registró la actividad de SPNs para comprobar la conexión sináptica entre neuronas PV+ y SPNs. El registro se realizó con la técnica de *patch clamp* en la configuración de célula completa en configuración de fijación de corriente o voltaje o bien en la configuración *cell attach,* en el mismo equipo utilizado para imagenología de calcio. Se utilizaron pipetas de borosilicato con una resistencia de 3-6 MΩ llenas de una solución que

contiene: KH_2PO_4 115 mM, $MgCl_2$ 2 mM, HEPES 10 mM, EGTA 10 mM, NaCl 10 mM, ATP 0.2 mM y GTP 0.2 mM, pH= 7.24, 290 ± 5 mOsm/L.

Análisis de datos

Los videos adquiridos fueron procesados con el software Im-Patch©. Se seleccionaron manualmente las células activas, como regiones de interés redondas (ROI, por sus siglas en inglés). Para seleccionar la actividad se calculó el cambio de fluorescencia ($\Delta F/F_0$) en donde ΔF es la media de los valores de los pixeles dentro de la ROI y F_0 es la media de la fluorescencia de un área circular de 20 pixeles alrededor de la ROI. Se calculó la primera derivada de esta señal, se consideraron cuadros activos aquellos en los que el valor de la derivada fue mayor a 2 desviaciones estándar, como se ha reportado previamente en el laboratorio (Pérez-Ortega *et al.*, 2016). A partir de esto se construyeron matrices binarias de actividad, en ella cada cuadro en el que una célula estuvo activa se coloca un 1 y los cuadros inactivos un 0. Las matrices fueron procesadas y analizadas en MATLAB para obtener:

- **Actividad de célula individual:** es el porcentaje de cuadros activos para cada célula en un periodo de tiempo. A partir de medir su actividad antes y después de la estimulación tomando 20% de la actividad promedio como umbral se clasificaron las neuronas en:
    - **Inhibidas**, neuronas activas antes de la estimulación que no presentan actividad después de esta.
    - **Deprimidas**, neuronas que presentan menor actividad después de la estimulación.

    - **Facilitadas**, neuronas que presentan mayor actividad después de la estimulación.
    - **Activadas**, neuronas que sólo muestran actividad después de la estimulación.
    - **Sin Cambio**, neuronas cuya actividad fue igual o el cambio fue menor al umbral.

- **Función de distribución acumulada** (CDF, por sus siglas en inglés): se construyó a partir de los valores de la actividad de cada célula, para comparar la actividad de las células individuales a través de diferentes secciones de un solo experimento. Las CDFs se realizaron para cada condición utilizando todas las neuronas de una muestra determinada.
- **Histogramas de coactividad:** es la suma de la actividad de todas las células por cada cuadro (imagen en un intervalo de tiempo) a lo largo del experimento, muestra cuantas neuronas se activaron juntas por cuadro. De esta medición obtenemos los picos de coactividad.
- **Actividad acumulada:** La cantidad de actividad neuronal por experimento se cuantificó mediante gráficos de actividad acumulada, que se construyeron sumando la actividad de todas las neuronas a lo largo del tiempo. Para comparar muestras de experimentos en la misma condición se hizo un ajuste lineal a los gráficos de actividad acumulada y se compararon las pendientes de estos ajustes.

- **Picos de coactividad significativos:** como un pico de coactividad lo conforman las neuronas que tuvieron actividad sincrónica o correlacionada en la misma ventana de tiempo, la significancia estadística de los mismos se determinó utilizando simulaciones de Montecarlo de las matrices de actividad, con 10,000 iteraciones cada una, sólo aquellos picos que superaron el umbral del azar se consideraron significativos.
- **Conexión funcional:** Para cada par de células se calculó 1-correlación de Jaccard y se tomó el 10% superior de los valores para asignar conexión.
- **Ensambles neuronales:** De acuerdo con las conexiones funcionales se agruparon las neuronas en ensambles usando el algoritmo rápido de comunidad (Newman, 2003) codificado por Buonova y Weck (2012).
- **Reconfiguración de ensambles:** Para calcular la reconfiguración, se generó una matriz de desconexión y a esta se le midió el coeficiente de agrupamiento (*clustering coefficient*).

Para comparar las CDF se utilizó la prueba Kolmogórov-Smirnov en MATLAB. La prueba de Montecarlo se realizó en MATLAB. Las pruebas de Wilcoxon, Pearson y Kruskal-Wallis se realizaron con el software Graph Prism.

Resultados

Received: 18 September 2019 | Revised: 23 December 2019 | Accepted: 2 January 2020

DOI: 10.1111/ejn.14670

SPECIAL ISSUE ARTICLE

EJN European Journal of Neuroscience FENS WILEY

Activation of parvalbumin-expressing neurons reconfigures neuronal ensembles in murine striatal microcircuits

Mariana Duhne[1] | **Esther Lara-González**[1,2] | **Antonio Laville**[1] | **Montserrat Padilla-Orozco**[1] | **Fatima Ávila-Cascajares**[1] | **Mario Arias-García**[1] | **Elvira Galarraga**[1] | **José Bargas**[1]

[1]División Neurociencias, Instituto de Fisiología Celular, Universidad Nacional Autónoma de México, México City, Mexico

[2]Facultad de Ciencias Químicas, Benemérita Universidad Autónoma de Puebla, Puebla, Mexico

Correspondence
José Bargas. División Neurociencias, Instituto de Fisiología Celular, Universidad Nacional Autónoma de México, México City 04510, Mexico.
Email: jbargas@ifc.unam.mx

Funding information
This work was supported by Consejo Nacional de Ciencia y Tecnología (CONACyT Mexico) Grant 251,144 (to E. G.), Dirección General de Asuntos del Personal Académico of the Universidad Nacional Autónoma de México (DGAPA-UNAM) Grants IN201517 and IN203020 (to E. G.), IN201417 and IN202920 (to J. B.).

Abstract

The striatum is the largest entrance to the basal ganglia. Diverse neuron classes make up striatal microcircuit activity, consisting in the sequential activation of neuronal ensembles. How different neuron classes participate in generating ensemble sequences is unknown. In control *mus musculus* brain slices in vitro, providing excitatory drive generates ensemble sequences. In Parkinsonian microcircuits captured by a highly recurrent ensemble, a cortical stimulus causes a transitory reconfiguration of neuronal groups alleviating Parkinsonism. Alternation between neuronal ensembles needs interconnectivity, in part due to interneurons, preferentially innervated by incoming afferents. One main class of interneuron expresses parvalbumin (PV+ neurons) and mediates feed-forward inhibition. However, its more global actions within the microcircuit are unknown. Using calcium imaging in ex vivo brain slices simultaneously recording dozens of neurons, we aimed to observe the actions of PV+ neurons within the striatal microcircuit. PV+ neurons in active microcircuits are 5%–11% of the active neurons even if, anatomically, they are <1% of the total neuronal population. In resting microcircuits, optogenetic activation of PV+ neurons turns on circuit activity by activating or disinhibiting, more neurons than those actually inhibited, showing that feed-forward inhibition is not their only function. Optostimulation of PV+ neurons in active microcircuits inhibits and activates different neuron sets, resulting in the reconfiguration of neuronal ensembles by changing their functional connections and ensemble membership, showing that neurons may belong to different ensembles at different situations. Our results show that PV+ neurons participate in the mechanisms that generate alternation of neuronal ensembles, therefore provoking ensemble sequences.

KEYWORDS

ensemble configuration, ensemble sequences, feed-forward inhibition, neuronal ensembles, parvalbumin-expressing neurons, striatal microcircuit

Abbreviations: CDF, cumulative distribution function; DA, dopamine; dSPNs, direct pathway spiny projection neurons; FSIs, fast-spiking interneurons; iSPNs, indirect pathway spiny projection neurons; NMDA, N-Methyl-D-aspartic acid; PBS, phosphate-buffered saline; PV+, parvalbumin-expressing interneuron; SPNs, striatal projection neurons.

Edited by Prof. Paul Bolam.

The peer review history for this article is available at https://publons.com/publon/10.1111/ejn.14670

1 | INTRODUCTION

Microcircuit dynamics consists in the sequential activation of neuronal ensembles that encode behaviour and neuromodulation (Carrillo-Reid, Hernández-López, Tapia, Galarraga, & Bargas, 2011; Carrillo-Reid et al., 2009; Jin, Tecuapetla, & Costa, 2014; Pérez-Ortega et al., 2016; Sheng, Lu, Shena, & Poo, 2019). Previous work reported the dynamics of spontaneous activity in striatal microcircuits: While intact slices are relatively silent, DA-depleted microcircuits show high overall activity monopolized by a dominant, highly recurrent ensemble (Carrillo-Reid et al., 2008; Jáidar et al., 2010, 2019; Pérez-Ortega et al., 2016). Low concentrations of NMDA or cortical stimulation in vitro produce alternating temporal sequences that go on for several minutes and transitorily release the circuit from the highly recurrent ensemble in dopamine (DA)-depleted striatal microcircuits (Aparicio-Juárez et al., 2019; Lara-Gonzalez, Duhne, Ávila-Cascajares, Cruz, & Bargas, 2019).

About 90% of striatal neurons are projection neurons (SPNs) (Gerfen & Surmeier, 2011; Graveland & DiFiglia, 1985), categorized as direct and indirect pathway neurons (dSPNs, iSPNs). Both types can belong to the same ensemble encoding learned tasks (Doig, Moss, & Bolam, 2010; Jáidar et al., 2019; López-Huerta et al., 2013; Surmeier, Carrillo-Reid, & Bargas, 2011; Tecuapetla, Jin, Lima, & Costa, 2016; Tecuapetla, Matias, Dugue, Mainen, & Costa, 2014) with specific spatiotemporal organization (Klaus et al., 2017), and neurons can belong to different ensembles encoding different tasks (Sheng et al., 2019).

The remaining 10% of the striatal neural population are interneurons of several kinds (Ibañez-Sandoval et al., 2010; Kawaguchi, Wilson, Augood, & Emson, 1995; Tepper & Bolam, 2004; Tepper & Kóos, 2017; Tepper, Tecuapetla, Koos, & Ibanñez-Sandoval, 2010; Wu, Richard, & Parent, 2000) among which PV+ fast-spiking interneurons (FSIs) are found. Previous studies have shown that cortical afferents preferentially innervate striatal FSIs (Arias-García et al., 2018; Assous & Tepper, 2019; Choi, Holly, Davatolhagh, Beier, & Fuccillo, 2019; Gittis, Nelson, Thwin, Palop, & Kreitzer, 2010; Kincaid, Zheng, & Wilson, 1998; Lee et al., 2019; Melzer et al., 2017; Pérez-Ortega et al., 2016; Ramanathan, Hanley, Deniau, & Bolam, 2002), which are more responsive than SPNs (Koós, Tepper, & Wilson, 2004; Mallet, Le Moine, Charpier, & Gonon, 2005; Parthasarathy & Graybiel, 1997; Tecuapetla, Carrillo-Reid, Bargas, & Galarraga, 2007). Each SPN receives synapses from 2–4 FSI (Rymar, Sasseville, Luk, & Sadikot, 2004; Tepper & Koós, 2017) given the extended axonal fields they possess (Straub et al., 2016; Tepper & Bolam, 2004). FSIs also connect with each other (Gittis et al., 2010; Kita, Kosaka, & Heizmann, 1990; Russo, Nieus, Maggi, & Taverna, 2013; Tepper & Koós, 2017), providing a mechanism to disinhibit or activate neighbouring ensembles (Assous et al., 2018; Lee et al., 2018; Roberts, White, Patton, Chen, & Mathur, 2019) through their feed-forward inhibition and filtering capabilities (Barroso-Flores, Herrera-Valdez, Lopez-Huerta, Galarraga, & Bargas, 2015; Beatty, Song, & Wilson, 2015; Gittis et al., 2010; Higgs & Wilson, 2019; Koós & Tepper, 1999; Koós et al., 2004; Mallet et al., 2005; Owen, Berke, & Kreitzer, 2018; Planert, Szydlowski, Hjorth, Grillner, & Silberberg, 2010). The key role of FSIs in proper microcircuit function is supported and confirmed by *in* vivo studies where inhibition or ablation of these neural population affects rodents' behaviour, burst firing, synaptic plasticity and learning (Gittis et al., 2011; Lee et al., 2018; Owen et al., 2018; Xu, Li, & Pittenger, 2016). Still, how PV+ fast-spiking interneurons (FSIs) may participate in microcircuit configuration of ensemble sequences remains unknown. For instance, their connectivity pattern and synchronizing or alternating capabilities (Berke, 2008, 2011; Buzsaki, 2010; Roberts et al., 2019; Russo et al., 2013) may allow ensemble configurations to be modified (Koós & Tepper, 1999).

Here, we make simple questions regarding FSI activation within striatal tissue in vitro to obtain categorical answers: what happens in the microcircuit after activation of a set of FSIs? Will most neurons be inhibited or disinhibited? Is the answer the same in resting non-stimulated circuits than in active stimulated ones? If ensembles may not be fixed but transient structures (Buzsaki, 2010), is it possible that FSIs activation leads to ensemble reconfiguration? These questions cannot be answered with different combinations of individual cell recordings. Therefore, we used calcium imaging and functional connectivity (Fröhlich, 2016) to address them.

2 | MATERIALS AND METHODS

Animal use and care. B6;129P2-*Pvalb*$^{tm1(cre)Arbr}$/J (JAX stock:017320, Hippenmeyer et. al., 2005) mice were acquired from Jackson Laboratories (https://www.jax.org/), and mating was carried out between homozygous mice. A total of 67 male and female animals were used for all experimental groups. Protocols were designed and performed as approved by the Institutional Committee for Laboratory Animals Care and Use of the Instituto de Fisiología Celular (IFC), UNAM (NOM-062-Z00-1999; laboratory protocols JBD-59-15) in accordance with the international norms for the ethical use of experimental animals established in the National Institutes of Health Guide for Care and Use of Laboratory Animals Eighth Edition (NIH, 2011). Mice were bred and housed in our animal facilities in a temperature-controlled, pathogen-free room, on a 12:12 light: dark cycle and allowed food and water intake ad libitum. Experimental samples were GCamp6f-tdTomato animals for electrophysiological recordings ($n = 6$ animals) and calcium imaging ($n = 20$ animals), ChR2-jRGECO for electrophysiological recordings ($n = 7$

animals) and calcium imaging ($n = 25$ animals), and control eGFP-jRGECO calcium imaging experiments ($n = 9$ animals). To prevent bias, mice from each litter were randomly chosen for different samples.

2.1 | Suppliers and reagents

Optogenetic and markers viral vectors were acquired as follows: pAAV-EF1a-double floxed-hChR2(H134R)-EYFP-WPRE-HGHpA was a gift from Karl Deisseroth (Addgene viral prep # 20298-AAV1; http://n2t.net/addgene:20298; RRID:Addgene_20298), pAAV.Syn.NES-jRGECO1b.WPRE.SV40, pAAV.Syn.Flex.GCaMP6f.WPRE.SV40 and pAAV.Syn.GCaMP6f.WPRE.SV40 were given by The Genetically Encoded Neuronal Indicator and Effector Project (GENIE) & Douglas Kim (Addgene viral prep # 100857-AAV1; http://n2t.net/addgene:100857; RRID:Addgene_100857; Addgene viral prep # 100837-AAV1; http://n2t.net/addgene:100837; RRID:Addgene_100837; Addgene viral prep # 100833-AAV1; http://n2t.net/addgene:100833; RRID:Addgene_100833, Dana et al., 2016). AAV pCAG-FLEX-tdTomato-WPRE and AAV pCAG-FLEX-EGFP-WPRE were a gift from Hongkui Zeng (Addgene viral prep # 51503-AAV1; http://n2t.net/addgene:51503; RRID: Addgene_51503; Addgene viral prep # 5102-AAV1; http://n2t.net/addgene:51502; RRID:Addgene_51502, Oh et al., 2014). NMDA (N-Methyl-D-aspartic acid, Sigma-Aldrich M3262- 100MG) and gabazine (2-(3-Carboxypropyl)-3-amino-6-(4 methoxyphenyl) pyridazinium bromide, Sigma-Aldrich S106-10MG) were purchased from Sigma-Aldrich. Antibodies were purchased as follows PV: (Abcam Cat# ab11427, RRID: AB_298032, https://www.abcam.com/) and Antirabbit Alexa Fluor 647 (Jackson ImmunoResearch Labs Cat# 711-605-152, RRID:AB_2492288) from Jackson Mice, Maine, US: https://www.jacksonimmuno.com/.

2.2 | Viral infection

Viral vectors were used to either co-express GCaMP6f-Syn-Flex and ChR2-eYFP or RGECO into PV+ neurons, or express tdTomato into PV+ neurons plus GCaMP6f under synapsin promoter for expression in all neurons. Co-expression dilutions were always 1:1. Mice PD: 30–35 were anesthetized by intraperitoneal injection of ketamine (85 mg/kg)-xylazine (15 mg/kg) solution. Stereotaxic surgery was performed injecting 0.5 μL of viral vectors (1:1 in co-expression transfection) in coordinates +0.8 mm AP, −1.7 mm LM and −3.0 mm DV from Bregma to a 0.1 μL/min rate with a dental needle. Mice were allowed recovery for 3 weeks. All in vitro experiments were carried out in mice PD: 56–61. Several measures were taken to minimize pain and discomfort. For stereotaxic surgery, artificial tears were placed in the mice's eyes to avoid damage. Body temperature was modulated peri- and post-operatively until animal full recovery.

2.3 | Immunohistochemistry

After electrophysiological recordings, slices were fixed with: Phosphate Buffer Saline (PBS) 4% PFA, 1% picric acid, pH = 7.4 and stored for immunohistochemistry. Slices were incubated with BSA 1% in PBS (pH = 7.2) for 30 min. They were washed with PBS for 10 min 3 times. Primary antibody was diluted 1:1,000 in PBS, triton 2.5% and applied for 24 hr. Slices were washed again for 10 min 3 times in PBS. Secondary antibody (1:500 in PBS/triton) was applied for an hour and a half, and later washed in PBS for 10 min 3 times. Slices were finally cover-slipped with DAPI-mounting medium (Vectashield, Vector Laboratories, Inc H-1200). Confocal images were acquired in a Zeiss LSM-710 (objective: C-Apochromat 20X N.A. 0.45, GCamp6f: 488 nm laser ex., 493–533 nm em; tdTomato: 543 nm laser ex., 565–615 nm em.; Alexa 647:633 nm laser ex., 658–704 nm em.; eYFP: 514 nm laser ex., 519–565 nm em.; RGECO: 543 nm laser ex., 586–630 em).

2.4 | Slice preparation

After being anesthetized by intraperitoneal administration of ketamine (85 mg/kg)-xylazine (15 mg/kg), mice were perfused intracardially with chilled sucrose solution (234 mM sucrose, 28 mM $NaHCO_3$, 7 mM dextrose, 4.54 mM pyruvate, 0.28 mM ascorbic acid, 2.5 mM KCl, 7 mM $MgCl_2$, 1.44 mM NaH_2PO_4, 0.4 mM $CaCl_2$ at 4°C). Brains were extracted and 250-μm-thick horizontal slices with a 30° angle were obtained in a vibratome (PELCO easiSlicer; Ted Pella, Redding, CA). Slices were then kept in artificial cerebrospinal fluid (126 mM NaCl, 15 mM dextrose, 26 mM $NaHCO_3$, 0.2 mM thiourea, 0.2 mM ascorbic acid, 2.5 mM KCl, 1.3 mM $MgCl_2$, 1.2 mM NaH_2PO_4, 2.0 mM $CaCl_2$, pH = 7.4; 300 ± 5 mOsm/L), perfused with 95% O_2 and 5% CO_2 at room temperature. Slices were placed under a 20X immersion objective (Olympus XLUMPLFLN Objective, 1.00 NA, 2.0 mm WD) while constantly perfused with ACSF and 95% O_2 and 5% CO_2 for electrophysiological and calcium imaging recordings.

2.5 | Electrophysiological recordings

PV+ neuron activity was recorded to confirm optogenetical stimulation specificity and cell integrity. SPNs activity was recorded to find PV+ neuron activation effects on them. In both cases, whole-cell current-clamp configuration was

carried out using patch pipettes (3–6 MΩ) filled with a solution containing 115 mM KH_2PO_4, 2 mM $MgCl_2$, 10 mM HEPES, 10 mM EGTA, 10 mM NaCl, 0.2 mM ATP and 0.2 mM GTP, pH = 7.24, 290 ± 5 mOsm/L.

2.6 | Calcium imaging recordings

Fluorophore stimulation was carried out with a Lambda HPX High power LED driver coupled to specific excitation emission filters as follows: GCamp6f: excitation BP460–480 nm, emission 495–540 nm (Olympus, U-MGFPHQ); tdTomato: excitation 565/20 nm (Chroma Technology Corporation, D565/20 m), emission 610/75 nm (Chroma Technology Corporation, HQ610/75m); and jRGECO: excitation 570/17 nm (Chroma Technology Corporation, ETS570/17 m), emission 590 LP (Chroma Technology Corporation, ET590lp). 2,160 frames recordings were obtained with a CoolSnap K4 camera, controlled by Im-Patch© open access software (www.impatch.ifc.unam.mx). PV+ neuron activity was observed using double expression of tdTomato-GCaMP6f and single GCaMP6f signal, and PV+ neuron activity was modulated by light stimulation in ChR2-jRGECO–double-infected mice. Light stimulation was applied (5 stimuli, 10 pulses at 40 Hz each) using 473 nm laser (CrystaLaser® 473 nm) coupled to a 200-nm optical fibre placed next to the slice. In other cases, electrical stimulation was administrated (5 stimuli, 10 pulses, 40 Hz, 1.1–1.3 mA.) via a bipolar concentric electrode (FHC, #CBCFE75) inserted in motor cortex layer V. A 15 mM KCl solution was administered at the end of all experiments to test slice viability; only those in which more than 85% of the cells were still viable were analysed.

2.7 | Data and statistical analyses

Electrophysiological and calcium imaging recordings were processed using Im-Patch© software and MATLAB© (RRID: SCR_001622, http://www.mathworks.com/products/matlab/). For calcium imaging recordings, single cells were identified and calcium transients were defined as $\Delta F/F_0$, where ΔF was the increase in fluorescence (F_i–F_0) over F_0, the background fluorescence: a time moving circle 25 pixels around the region of interest (ROI). The positive portion of the time derivative, $d(\Delta F/F_0)/dt$, was taken as a proxy of neuronal firing for any given cell as long as it surpassed 2.5 standard deviations from the basal signal (Pérez-Ortega et al., 2016).

Activity matrices were built for any given cell where 1 accounted for an active frame and 0 for a non-active frame. Matrices were analysed in MATLAB to extract population activity with single-cell resolution. Population activity per experiment was quantified using cross-correlated activity between every pair of cells, frame by frame, along time (see below). Histograms below raster plots used column vectors addition of cell activity frame by frame. Cumulative cellular activity is the addition of these vectors along time, linear fits were approximated to this activity and their slopes were used in box plots to compare different experimental conditions (Aparicio-Juárez et al., 2019). Wilcoxon matched-pairs test was used to compare cellular activity before and after light stimulation. Cumulative distribution functions (CDFs) added cells from whole samples in each experimental condition. It was calculated using the percentage of active frames: briefly, the number of active frames was divided by the total number of frames and multiplied by 100. Kolmogorov–Smirnov test was used to compare CDFs. We then classified neurons according to their activity that is the percentage of active frames before and after stimulation. To assign functional connections, for every pair of cells 1-Jaccard correlation coefficient was calculated using MATLAB. The threshold to assign functional connections was 90%. Significant differences between functional connection distribution of shuffled data and experimental data were found after 90%. In this way, neurons that were commonly active together were grouped into neuronal ensembles using the fast community algorithm (Newman, 2003) coded by Bounova and de Weck (2012).

3 | RESULTS

3.1 | Calcium imaging of PV+ neurons

Adenoviral infection (tdTomato) was used to identify PV+ neurons (Figure 1a first frame from left to right; see Material and Methods). Additional adenoviral infection using GCaMP6f under the synapsin promoter identified surrounding neurons (Figure 1a second frame). Third frame in Figure 1a shows that tdTomato labelled neurons were also immunoreactive to PV antibodies. Last image shows the merge of all previous frames. Firing of neurons identified in this way commonly displayed non-linear current-spiking relations showing short stuttering bursting or continuous non-adapting high-frequency firing upon depolarizing current injections of increasing intensity (Figure 1b; Sciamanna & Wilson, 2011). In spite of their polarized resting potentials (Arias-García et al., 2018) some PV+ neurons were spontaneously active (Berke, 2011; Mallet et al., 2005; Rendón-Ochoa et al., 2018). Simultaneous electrophysiological and calcium imaging recordings of identified and spontaneously active neurons (Figure 1c and see below) show that firing is commonly detected by the positive time derivative of the associated calcium entry ($d(\Delta F/F_0)/dt$). However, this method underestimates continuous high-frequency firing indicating only the onset (Roberts et al., 2019). Taking this caveat in mind, it is fair to say that this type of

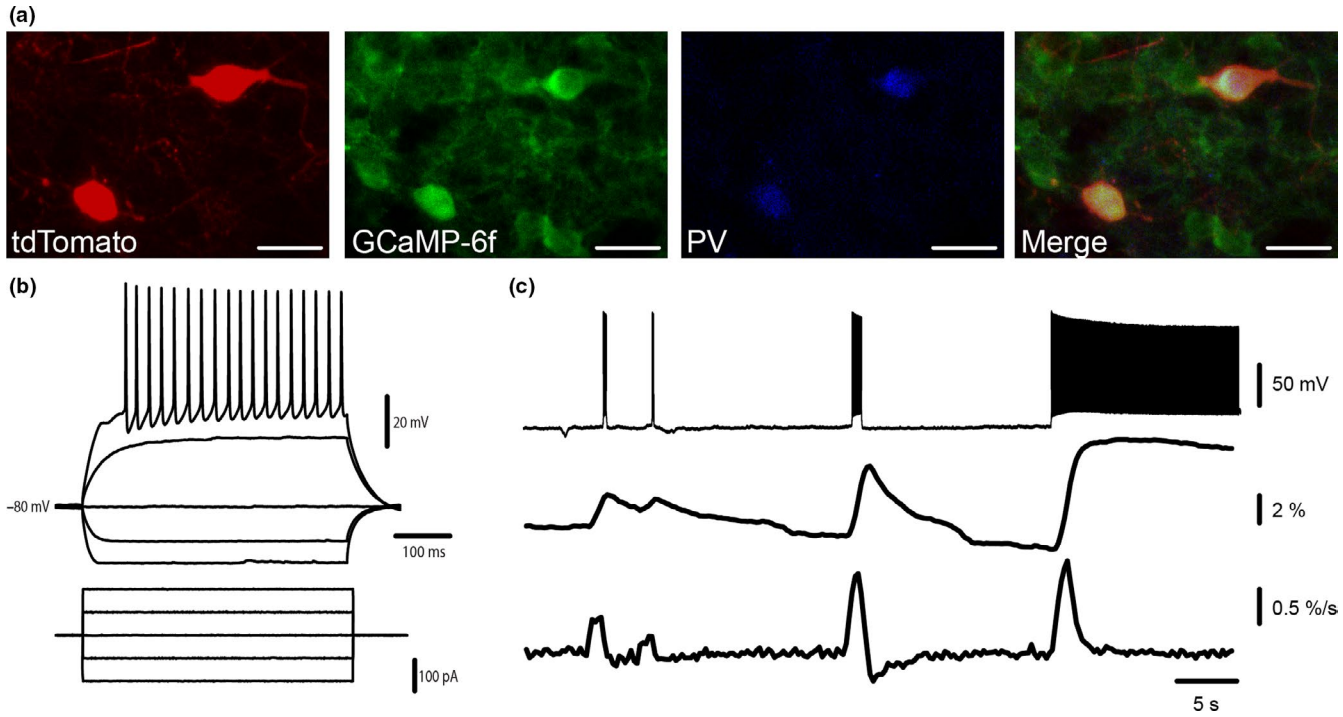

FIGURE 1 Simultaneous electrophysiological and calcium imaging recordings of PV+ neurons. (a) Panels from left to right show: first, a confocal micrograph of PV+ neurons expressing tdTomato, second, the same field with several neurons expressing GCaMP6f (synapsin promoter), third, PV immunoreactive neurons, finally, a merge of the preceding images. Scale bar = 20 μm. (b) Voltage responses and action potential firing of an identified PV+ neuron (top) in response to depolarizing and hyperpolarizing intracellular current injections of different magnitudes (current-clamp in whole-cell configuration). (c) Simultaneous recording of the spontaneous firing (top) and its corresponding calcium transients ($\Delta F/F_0$; middle) of a PV+ neuron. The bottom trace is the first time derivative of the calcium transients ($d(\Delta F/F_0)/dt$). The positive component matches neuronal firing although it only reports the onset in the case of a continuous spike train

firing is hard to observe spontaneously (Sharott, Doig, Mallet, & Magill, 2012) due to a mixture of intrinsic membrane properties and synaptic noise (Higgs & Wilson, 2019).

3.2 | PV+ neurons account for 6%–10% of functional neurons in the active striatal microcircuit

An adequate cortical stimulus may activate the striatal microcircuit during several minutes and the same result is obtained after bath addition of 2 μM NMDA (Lara-Gonzalez et al., 2019). PV+ neuron activity was evoked in the striatal microcircuit after cortical stimulation (schematized in Figure 2a). Figure 2b shows that PV+ neurons account for the 6%–11% of active neurons across all experiments ($n = 17$), differing from the 0.7%–1% reported anatomically (Luk & Sadikot, 2001; Rymar et al., 2004; Tepper & Bolam, 2004), suggesting a higher activity ratio for PV+ neurons than for SPNs or other PV− neurons. This technique allowed us to record the activity of several PV+ interneurons simultaneously over brief periods of time. About 54% of all PV+ neurons identified in our experiments displayed spontaneous activity, and the rest were only active when depolarized by the addition of KCl at the end of the experiment. When looking at activity per frame across PV+ and PV− neurons, no significant differences in CDFs of cell activity were found (Figure 2c). Approximately, 60% of PV+ neurons have sparse activity: 5% or less frames showed activity (Figure 2c). Therefore, multirecording allows to observe spontaneous firing in PV+ neurons even if sparse. Figure 2d shows a raster plot from a representative experiment. Dots in each row of the raster plot show the activity of single neurons along time. Red dots denote PV+ neurons. Histogram of correlated activity bellow the raster plot shows no special participation of PV+ neurons into significant activity peaks. No correlation of active frames between PV+ neurons or between PV+ and PV− neurons was found (Berke, 2011). We conclude that firing of PV+ neurons was heterogeneous and that no special relationship among the different classes of neurons was found in the striatal freely running microcircuit.

3.3 | PV+ neurons do inhibit striatal projection neurons individually

Figure 3a left panel shows a confocal micrograph of ChR2-eYFP-expressing PV+ neurons (see Material and Methods).

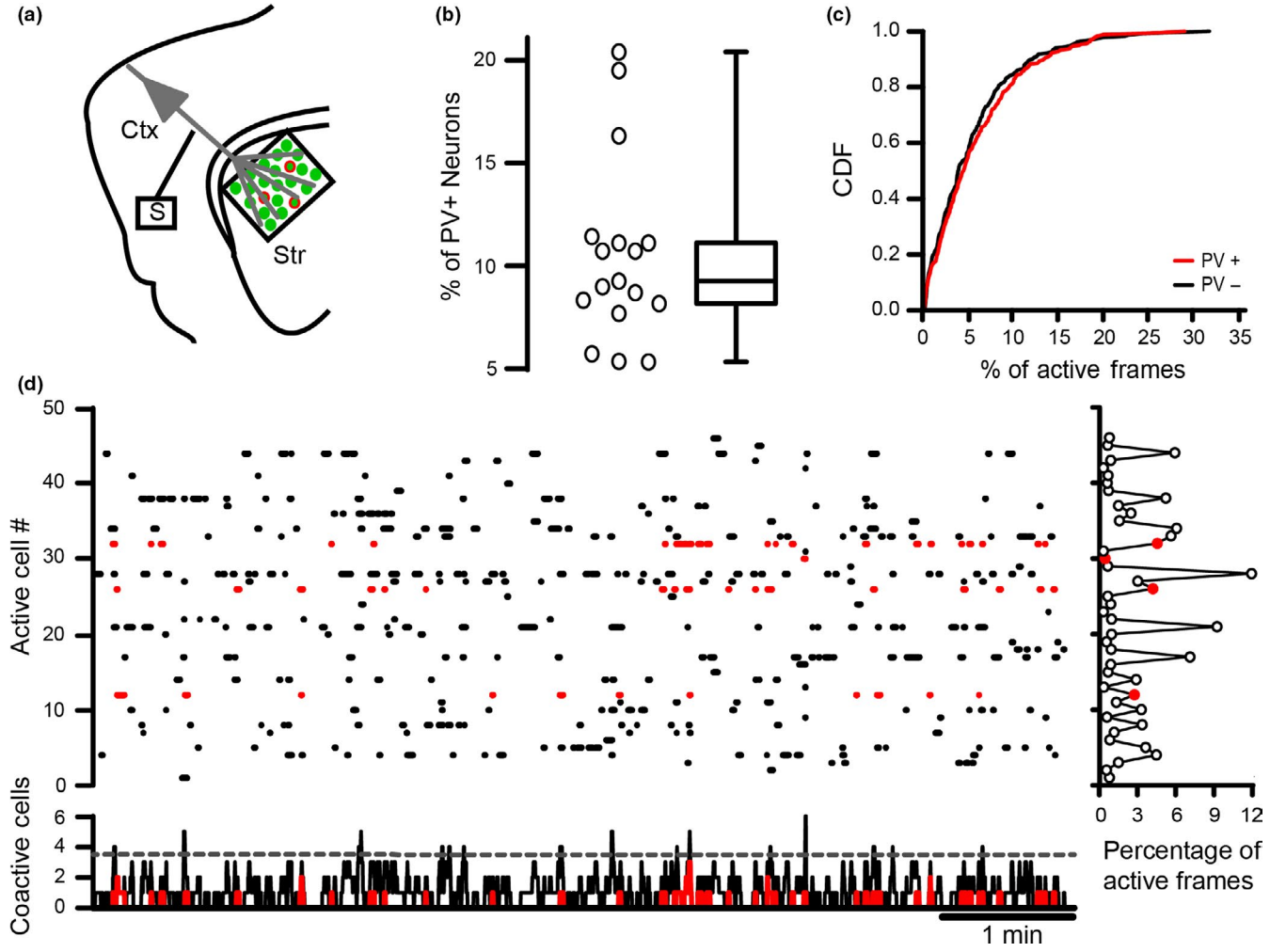

FIGURE 2 Heterogeneous participation of PV+ neurons in cortical stimulated striatal microcircuit activity. (a) Schematic representation of the recording and stimulation protocol. Calcium imaging recordings were acquired in the striatum after cortical stimulation in cortex layer V (Aparicio-Juárez et al., 2019). (b) Box plot showing median and quantiles of PV+ neurons active per experiment ($n = 17$ experiments). (c) Cumulative distribution functions of cellular activity (activity/time) for both PV+ and PV− neurons. No statistical difference was found (PV+ $n = 153$, PV− $n = 261$; Kolmogorov–Smirnov test). A heterogeneous and not a conspicuous pattern of activity between PV+ neurons or between PV+ and PV− neurons was observed, despite the presence of significant coactivity peaks (Berke, 2011). (d) An adequate cortical stimulus activates the striatal microcircuit during several minutes, and the same result was obtained after bath addition of 2 μM NMDA (Lara-Gonzalez et al., 2019). A representative raster plot where dots in each row represent the activity of a different neuron is shown. Red dots denote identified PV+ neurons. Histogram below shows the number of active neurons at a given time, and red bars indicate PV+ neurons activity. Histogram at right shows activity of each neuron normalized as percentage of active frames. Note heterogeneity of PV+ neurons firing in these conditions. Dotted line in the histogram indicates the presence of statistically significant peaks of correlated neuronal activity ($p < .05$)

Second panel (from left to right) shows neighbour neurons transfected with jRGECO under the synapsin promoter. Third panel confirms that ChR2-eYFP-expressing neurons are immunoreactive to PV antibodies. Last panel is the merge of all images.

Figure 3b illustrates current-clamp whole-cell recordings of an identified ChR2-eYFP+ neuron showing voltage responses to both depolarizing and hyperpolarizing current injections. Non-adapting trains of high-frequency firing with narrow spikes and deep after hyperpolarizations are observed (FSI; e.g. Arias-García et al., 2018). Blue light pulse (15 ms, 473 nm) stimulates the firing of identified eYFP+ neurons expressing ChR2. Photo-depolarized neurons fired brief trains of action potentials (spikes look broader because 5–6 responses were averaged). A pulse of green light (15 ms, 570/17 nm; jRGECO stimulation wavelength) did not elicit a firing response ($n = 8$ cells). The same experiment was performed in voltage-clamp mode showing a similar result: unclamped action currents were elicited with blue light but not with green light (Figure 3d, $n = 8$ cells). Additionally, SPNs firing was evoked with a depolarizing current pulse before (Figure 3e black trace) and after stimulating ChR2-eYFP+ neurons with a blue light stimulus (Figure 3e blue trace; 5 ms blue light pulses

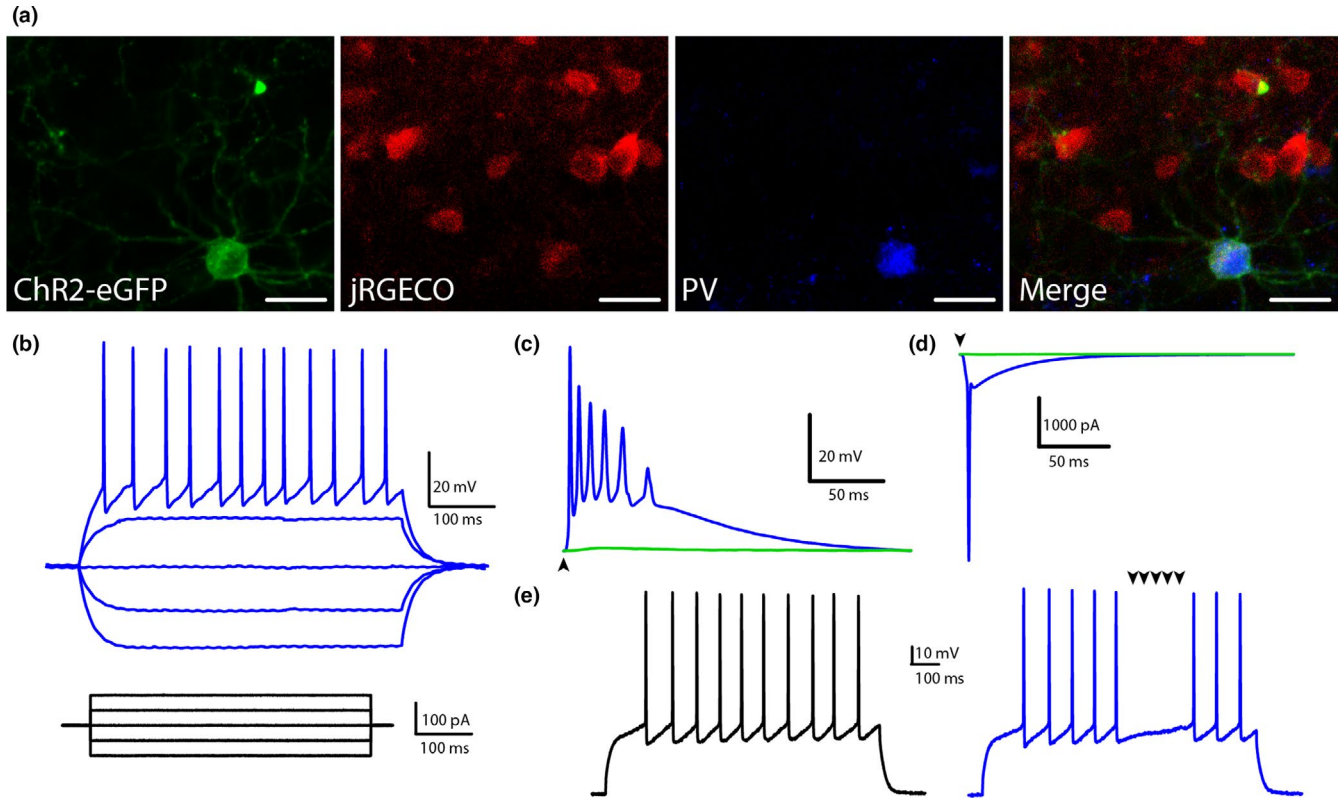

FIGURE 3 Inhibition of striatal projection neurons during optogenetic stimulation of PV+ neurons. (a) Panels from left to right show: first, a confocal micrograph of ChR2-eYFP-expressing PV+ neuron, and second, neurons in the same field identified by jRGECO (synapsin promoter). ChR2-eYFP allows optostimulation of PV+ neurons with blue light without interfering with microcircuit calcium imaging. jRGECO allows calcium imaging of the microcircuit with a green light stimulus. Third panel shows that ChR2-eYFP-expressing neuron is PV immunoreactive. Finally, the merge of previous images is shown. Scale bar = 20 μm. (b) Voltage responses (top) of a PV+ neuron to hyper- and depolarizing intracellular current injections (bottom). (c) Averaged voltage response to a pulse of blue light (15 ms 473 nm; blue trace) of a PV+ ChR2-eYFP-expressing neuron. The same neuron did not respond to a pulse of green light (570/17; green trace, $n = 8$ cells) of the same duration (jRGECO stimulation wavelength). Spikes seem broad due to jittering of averaged traces. (d) A similar experiment in somatic voltage-clamp conditions. Arrowheads indicate light stimulation in c and d. (e) The black trace shows firing of a SPN evoked with a depolarizing intracellular current injection of 200 pA (not shown). Blue trace: when PV+ neurons are activated with light (arrowheads: 5 ms blue light 20 Hz pulses). SPN firing is prevented ($n = 7$ cells)

at 20 Hz, $n = 7$ cells). It is shown that SPNs firing stops during PV+ neuron stimulation with a light stimulus (more detailed differences between FSIs and SPNs firing can be seen in Arias-García et al., 2018). These results are similar to those found by other authors and prove that photostimulation of FSIs inhibits SPNs (refs. in: Tepper & Koós, 2017). These actions could be blocked by the addition of gabazine and were also observed in on-cell patch recordings (Data not shown). In view that FSI inhibition is so reliably on single SPNs, one question is why their action cannot be discerned in freely running active microcircuits where several PV+ neurons can be demonstrated to be firing. Therefore, to better observe PV+ neuron actions we decided to photostimulate them while observing dozens of neurons simultaneously using calcium imaging, as groups of PV+ neurons may form a syncytium or network that may exert a powerful inhibition across the circuit (Roberts et al., 2019; Russo et al., 2013; Tepper & Koós, 2017).

3.4 | PV+ neuron actions on resting non-stimulated striatal microcircuits

Once observed that light activation of PV+ neurons inhibits the firing of individually recorded SPNs, we decided to test PV+ neuron actions at the microcircuit level. Figure 4a shows the raster plot of a representative experiment in which dots in each row represent the activity of single neurons (*y*-axis) along time (*x*-axis), 6 min before and 12 min after a light stimulus was delivered to the preparation (see arrow on top; 5 trains of 10 pulses each, 5 ms pulse duration, at 40 Hz, 473 nm or blue light). Single neuron positions in the y-axis were sorted so that those neurons active before light stimulus appeared together (left of raster plot). In this condition, very few neurons are spontaneously active (about 15 neurons in this case; Lara-Gonzalez et al., 2019). Histogram at bottom shows correlated neuronal firing. Green bars add the activity of PV+ neurons that responded to the stimulation.

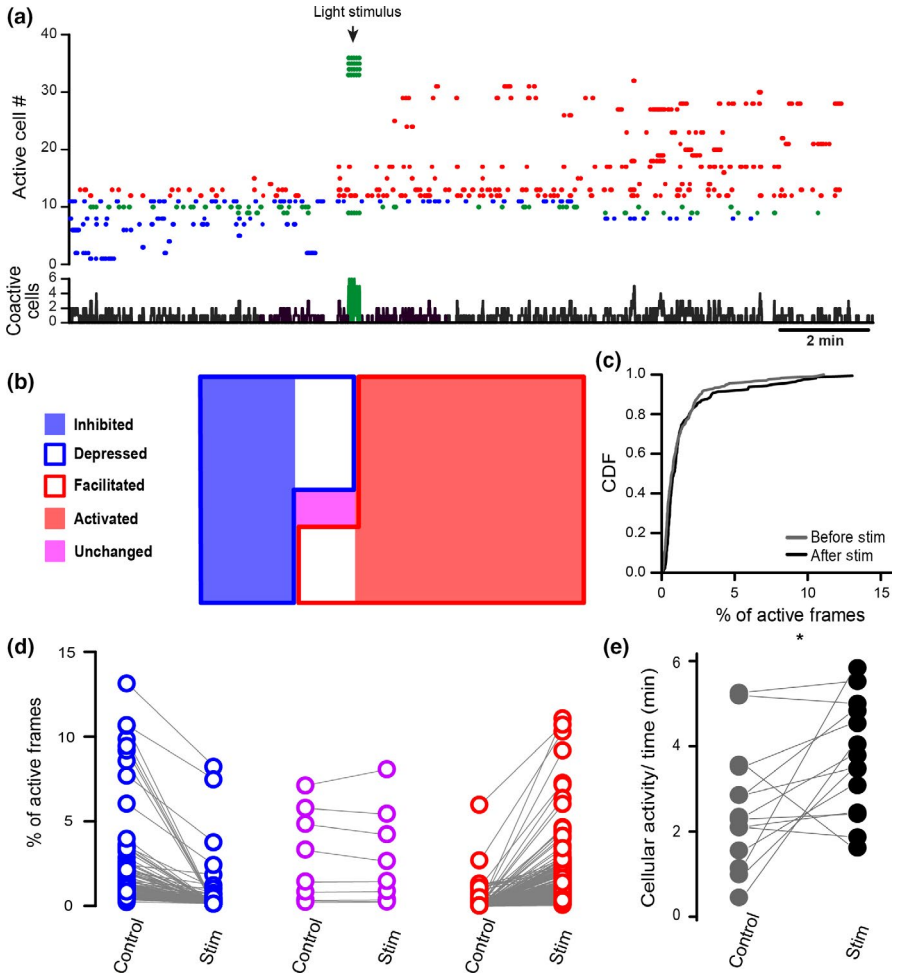

FIGURE 4 Inhibition and activation of spontaneous striatal activity after optogenetic stimulation of PV+ neurons. (a) Representative raster plot shows scarce activity prior to light stimulation (arrow on top, 5 trains of 10 5 ms pulses at 40 Hz, 473 nm). After PV+ (green dots) stimulation some neurons in the microcircuit increase their activity (red dots) while others decreased it (blue dots). Histogram below shows neuronal coactivity along time. Green bars denote stimulus-related PV+ neuron activity. (b) A sample of neurons ($n = 14$ experiments; $n = 400$ cells) classified by activity change is illustrated with a Venn diagram. For neurons active from the beginning activity would increase (facilitated, empty red square; $n = 24$), diminish (depressed, empty blue square; $n = 32$), totally disappear (inhibited, filled blue square; $n = 97$) or remain unchanged (magenta square; $n = 9$), while some neurons initially silent became active after light stimulation (activated, filled red square; $n = 238$). (c) CDF plots showing cumulative neuronal activity along time (% of active frames), before (grey line) and after light stimulation (black line) were significantly different (Kolmogorov–Smirnov test, $p = .0166$; $n = 400$ neurons). (d) Facilitated (red circles) and depressed (blue circles) categories were based on 20% activity increase or decrease, or no change (magenta) using all experiments. (e) The comparison of cumulative total cellular activity (total activity/time; see Aparicio-Juárez et al., 2019) before and after the light stimulus was significantly different (Wilcoxon's *t* test; $n = 14$ experiments; $p = .0166$) and mostly increasing

The stimulation protocol evokes single action potentials (see Figure S1). After PV+ neuron stimulation, most experiments showed that more neurons were activated than those inhibited. This counter-intuitive result (as PV+ neurons are inhibitory) had been predicted in a model of the striatal microcircuit with background input (Humphries, Wood, & Gurney, 2009). The raster plot (Figure 4a) is coloured as follows: blue dots denote neurons whose activity was significantly inhibited or depressed after PV+ neuron stimulation, red dots indicate those neurons that were facilitated or become active after PV+ neuron stimulation and green dots denote PV+ neuron activity. The actions of PV+ neuron stimulation were consistent ($n = 14$ experiments and $n = 400$ neurons in total): some neurons increased their activity (facilitated; $n = 24$) or reduced their activity (depressed; $n = 32$), while others silent in the control became active (activated; $n = 238$) and some initially active became silent (inhibited; $n = 97$). Only $n = 9$ neurons (2%) were unaffected (Figure 4b). That is, most neurons in the network were affected by PV+ neuron activation, which resulted in more active neurons than before. We performed similar experiments stimulating direct and indirect pathway striatal projection neurons (dSPNs and iSPNs), which are important to evoke lateral inhibition (Czubayko & Plenz, 2002; see Figure S2); nonetheless, we did not observe significant

long-lasting changes in network behaviour. However, other neuron types and stimulation protocols need to be tested in the future. We can infer that PV+ neurons help ignite activity in a resting microcircuit by disinhibition, although some neurons are actually inhibited. In fact, PV+ neurons active before the stimulus were among depressed neurons, confirming that they may inhibit each other and produce ensemble alternation (Russo et al., 2013). Examples of calcium transients of different PV+ neurons are shown in Figure S3. A significant difference in the CDFs of cell activity before and after the stimulus quantified the action of PV+ neurons upon the microcircuit (Figure 4c; $n = 400$ neurons; $p = .0166$, Kolmogorov–Smirnov test). Figure 4d shows paired plots to illustrate activity reduction (both depression and inhibition; blue circles), activity increase (both activation and facilitation; red circles) and unaffected neurons. Finally, cumulative cellular activity/ time ratio was quantified for all experiments (Figure 4e). There is a significant increase in cumulative cell activity after PV+ neuron stimulation (11 out of 14 experiments; $p = .0166$, Wilcoxon's t test). As PV+ neurons may receive a preferential innervation from the cortex (Arias-García et al., 2018; Assous & Tepper, 2019; Choi et al., 2019; Gittis et al., 2010; Kincaid et al., 1998; Lee et al., 2019; Melzer et al., 2017; Ramanathan et al., 2002), it is inferred that they can amplify cortical commands when a microcircuit is being activated, that is they not only serve as feed-forward inhibitors.

3.5 | PV+ neuron actions on active stimulated striatal microcircuits

Because PV+ neurons may help to differentially activate or inhibit neurons in a resting microcircuit, we then asked how PV+ neurons act on already ongoing microcircuits. Raster plot in Figure 5 illustrates the optogenetic activation of PV+ neurons (arrow) in a striatal microcircuit activated by the addition of 2 μM NMDA (Carrillo-Reid et al., 2011; Lara-Gonzalez et al., 2019). In this case (Figure 5a), 3 PV+ neurons were initially active (green dots) from a total of 50 neurons (6%). Light stimulus activated other 2–3 PV+ neurons (green bars in coactivity histogram below; photostimulated neurons are not depicted in the raster plot). Counting neurons from ($n = 8$) similar experiments yielded: $n = 219$ neurons were depressed or inhibited (blue), $n = 182$ neurons were facilitated or activated (red) and $n = 155$ neurons were unaffected after PV+ stimulation ($p = .0038$; Pearson's chi-squared test). These results suggest that under activated conditions neuron groups that are depressed are significantly larger than those facilitated. Raster plots showed significant peaks of correlated activity ($p < .05$), and alternation between neuronal ensembles (Perez-Ortega et al., 2016) was verified: while some ensembles are inhibited, others are activated in sequence. To corroborate the action of PV+ neurons in circuit activity, we compared them with and without PV+ neuron optostimulation (Figure 5b). Dashed line boxes indicate experiments ($n = 8$) that identified but did not stimulate PV+ neurons while solid line boxes denote experiments where PV+ neurons were identified and optostimulated ($n = 8$). In this case, unaffected neurons by stimulated neurons were not significantly different ($p = .23$). However, depressed or inhibited neurons in the active sample were significantly more ($p = .0011$), while facilitated or activated neurons were significantly less ($p = .0019$) when PV+ neurons were activated, confirming that in already active circuits PV+ neurons act more in agreement with their inhibitory role, examples of calcium transients of PV+ neurons are shown in Figure S4. NMDA and cortical stimulated microcircuits yielded equivalent results (Lara-Gonzalez et al., 2019). To conclude, these results show that PV+ neurons participate both in the inhibition and probably disinhibition that take place during the alternation of neuronal ensembles that generate temporal sequences (see Discussion). If this is true, one prediction would be that some functional connections between circuit neurons may transiently disappear while others are created when groups of PV+ neurons are activated.

3.6 | PV+ neuron stimulation changes functional connectivity

Given that groups of neurons are inhibited while others are facilitated after PV+ neuron stimulation, the effect of PV+ neurons on functional connectivity was evaluated. Neurons were grouped according to their cross-correlated activity before and after the stimulation of PV+ neurons (5 trains of 10 pulses at 40 Hz, Figure 6a). There were neuronal ensembles before and after PV+ neuron stimulation, and in both cases, there were significant peaks of correlated activity. However, these neuronal ensembles and their functional connections were different (shown by different colours) showing that PV+ neuron stimulation not only modifies neuronal activity by inhibiting and activating different neuronal groups but also modifies their ensemble membership. This outcome was consistent along all experiments ($n = 8$). Additionally, circular visualizations of functional connectivity between ensemble changes (Figure 6b) and columns at the middle show that several neurons change their companions after PV+ neuron activation. A pie plot (Figure 6c) shows that some functional connections were lost (50%), while others were formed (42%), and a few were preserved (8%), confirming that the organization of the microcircuit had changed ($n = 2{,}641$ connections from $n = 8$ experiments). This reconfiguration of ensembles was significant (Figure 6d) and depended on PV+ neuron stimulation ($p = .0357$; Kruskal–Wallis test; measured as the reciprocal of the clustering coefficient). Also, CDFs of ensemble reconfiguration after PV+ neuron stimulation were also significant when taking the neurons from all experimental

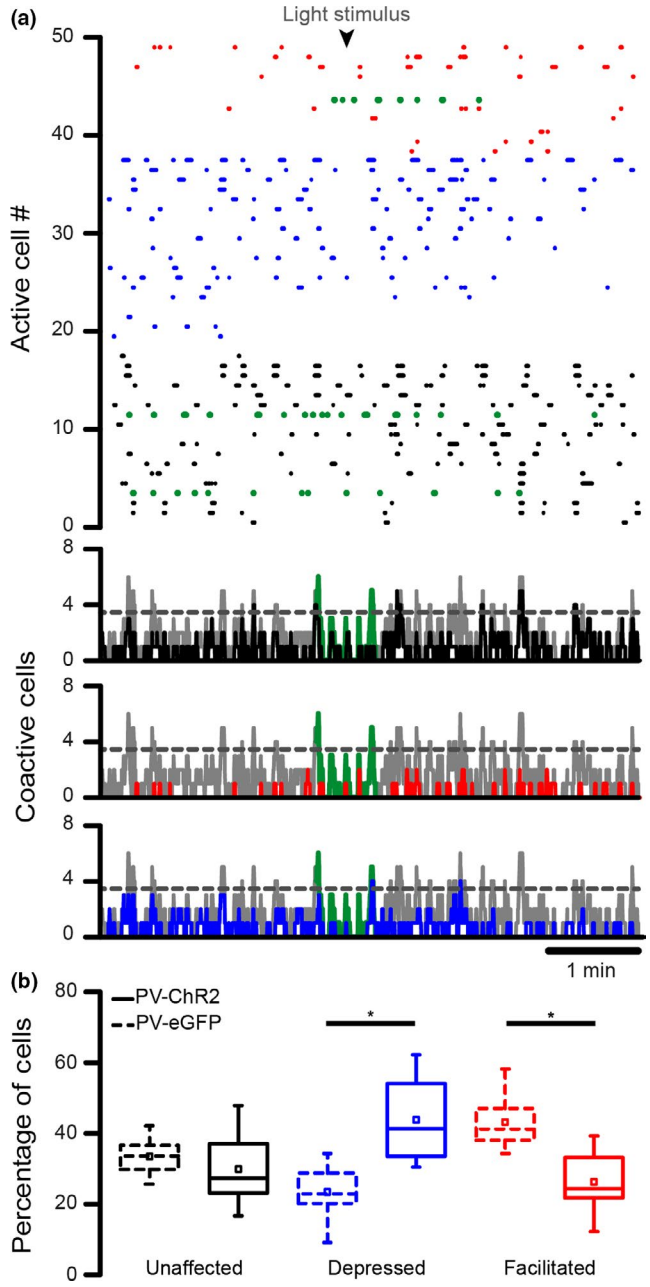

FIGURE 5 Activation of PV+ neurons within a striatal microcircuit operating by the addition of NMDA. (a) Sorted raster plot of a representative striatal microcircuit after being activated by the addition of 2 μM NMDA. Blue light stimulation was applied at the arrowhead. As in Figure 4, cells activity was coloured according to their change after light stimulation: depressed (blue; $n = 219$; $n = 8$ experiments), facilitated (red; $n = 182$) and unchanged (black; $n = 155$). In contrast to non-stimulated resting microcircuits, where facilitated cells were the majority (Figure 4), in active microcircuits depressed cells were more abundant ($p = .0038$; Pearson's chi-squared test), as shown in representative activity histograms at bottom ($n = 8$ similar experiments). Green dots denote PV+ neurons, and their correlated activity during stimulation is indicated by green bars (stimulus-associated PV+ neurons were erased from the raster plot). Dotted lines in the histogram indicate that some peaks of correlated neuronal activity were significant ($p < .05$), denoting the presence of ensemble sequences (Pérez-Ortega et al., 2016). (b) Box plots showing the percentage of cells per experiment classified into different populations: dashed boxes indicate that PV+ were identified but were not optostimulated (control, $n = 8$ experiments), and solid line boxes indicated that PV+ neurons were identified and photostimulated ($n = 8$ experiments). The percentage of neurons that did not reduce or increase their activity (unaffected) after the stimulus were not significantly different when comparing both samples ($p = .23$; NS). However, in optostimulated tissue, neurons that reduced their activity (depressed) were significantly more ($p = .0011$), and a significantly less number of neurons increased their activity after the stimulation (facilitated, $p = .0019$), meaning that in already active microcircuits activation of PV+ interneurons produce more expected changes: a similar number of neurons were depressed or facilitated in their firing. NMDA and cortical stimulated microcircuits yield equivalent results (Lara-Gonzalez et al., 2019)

samples: control using PV-eGFP ($n = 476$ neurons); PV+ neuron stimulation or PV-ChR2 ($n = 556$ neurons), $n = 8$ experiments in each case ($p = .0008$; Kolmogorov–Smirnov test). We conclude that incoming cortical and thalamic commands use PV+ neurons to choose which neurons belong to which ensemble when task or environment change (e.g. Sheng et al., 2019), while using many of the same neurons.

4 | DISCUSSION

The following original observations were obtained from the experiments in the present work. (a) When active striatal microcircuits are observed in brain slices in vitro, some identified PV+ neurons have spontaneous activity. This activity is heterogeneous, some neurons firing at higher frequency than others. (b) When optogenetically stimulated in resting, non-stimulated microcircuits, PV+ neurons activated more neurons than those inhibited, similarly to cortical stimulation itself (Aparicio-Juárez et al., 2019; Lara-Gonzalez et al., 2019). (c) When the striatal microcircuit is active and exhibits ensemble temporal sequences, activation of a set of PV+ neurons results in both inhibited and activated neurons. (d) Activation of PV+ neuron groups may select which ensembles of SPNs can conform the encoding of certain network states (Pérez-Ortega et al., 2016) in agreement with their corresponding motor sequences in in vivo experiments (Sheng et al., 2019). In support of these observations, we show that activation of PV+ neurons can reconfigure neuronal ensembles by using some of the same neurons but changing their functional connections and their partners.

4.1 | Spontaneous firing of striatal PV+ neurons in vitro

Calcium imaging has been used extensively to study neuronal microcircuit activity (Aparicio-Juarez et al., 2019;

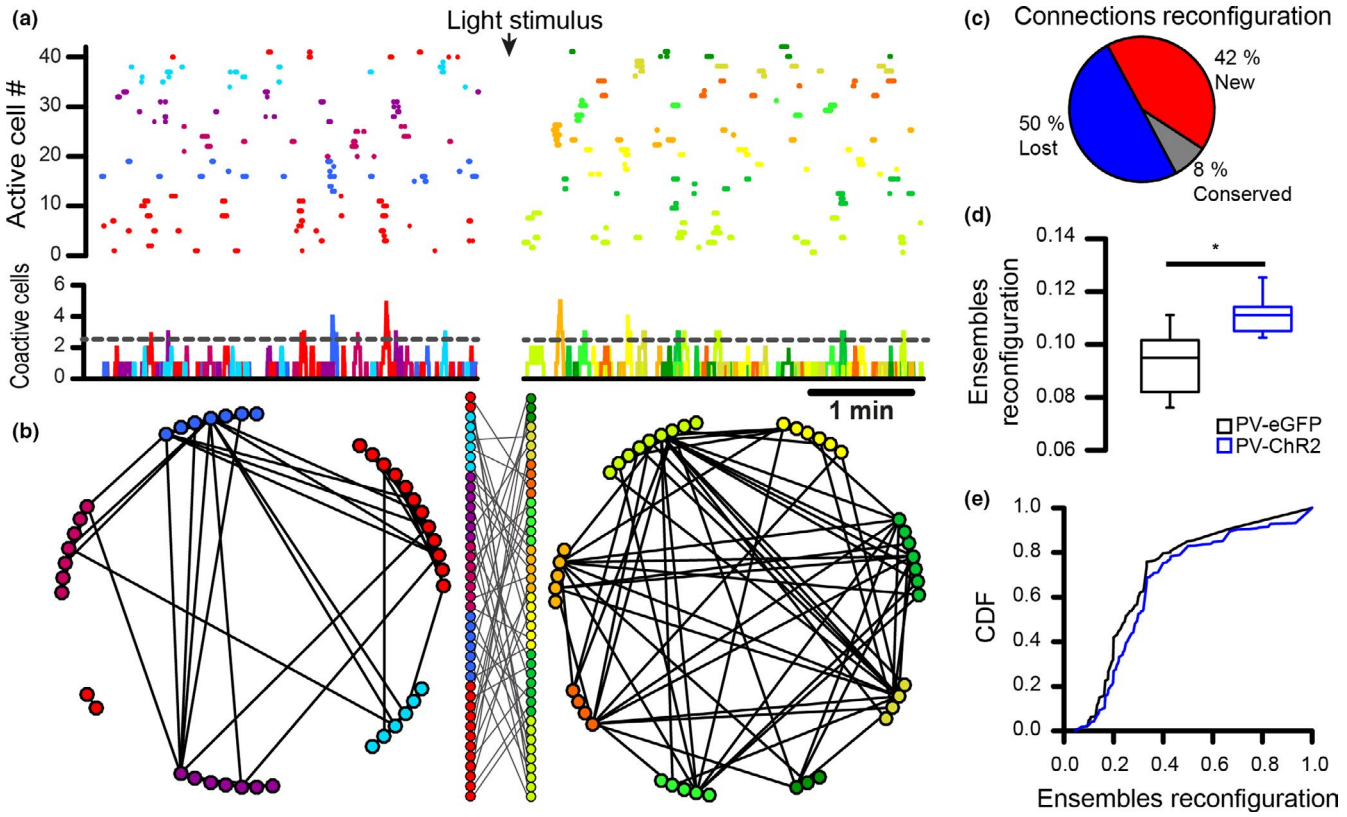

FIGURE 6 Activation of PV+ neurons reconfigures neuronal ensembles in the activated striatal microcircuit. (a) As previously shown, diverse grouping methods can show statistically significant peaks with correlated firing forming neuronal ensembles that alternate their activity in the striatal microcircuit activated by 2 μM NMDA. Here, groups of coactive cells were separated by their cross-correlated activity. Different colours denote different ensembles. Bottom histograms show peaks of correlated activity. (b) Circular visualization of ensemble functional connectivity during NMDA microcircuit activation. After optogenetic stimulation of PV+ neuron (top arrow) groups of correlated neurons change their component elements (indicated by different colours). However, the new ensembles keep generating significant coactivity peaks: histogram at the bottom. Newly formed ensembles show a different pattern of functional connections. Centre in B: new ensembles were formed by the same neurons, which changed some of their companions and connections assembling different groups, that is, the microcircuit was partially reconfigured by PV+ neuron activation. (c) Pie plot shows changes in functional connectivity: some connections are lost while new ones are created, and few are preserved ($n = 2{,}641$ connections from 8 experiments). (d) Ensemble reconfiguration comparing circuits without and with PV+ neuron stimulation ($p = .0357$; Kruskal–Wallis test; measured as the reciprocal of the clustering coefficient). (e) Cumulative distribution functions of cell reconfiguration before and after stimulation using all cells from all experiments: Control (PV-eGFP) $n = 476$ cells; PV+ stimulated (PV-ChR2) $n = 556$ cells, $n = 8$ experiments in each case ($p = .0008$; Kolmogorov–Smirnov test)

Carrillo-Reid et al., 2008; Perez-Ortega et al., 2016; Sheng et al., 2019). Here, we asked how PV+ neuron activation changed striatal microcircuit dynamics by identifying these interneurons in transgenic mice and activating them with ChR2. Simultaneous electrophysiological recordings and calcium imaging showed that calcium imaging may underestimate PV+ neuron activity when they fire continuously at a high rate (Chen et al., 2014; Roberts et al., 2019). However, this firing is rarely found spontaneously (Sharott et al., 2012) possibly by the interaction between intrinsic membrane properties and synaptic entries (Higgs & Wilson, 2019). Even if underestimation of activity by calcium imaging has been documented for other interneurons (Rehani et al., 2019), a further underestimation of PV+ neuron activity may come from the mice strain used: PV-IRES-Cre line has lower penetrance in comparison with the PV-2A line (Madisen et al., 2010; Owen et al., 2018). However, in spite of the above constraints, participation of PV+ neurons in the active microcircuit amounted to 5%–11% with outliers approaching 20% even if, anatomically, they account for less than 1% of the neurons in the circuit. We conclude that their activity in the network is higher than that of PV− neurons, most of them SPNs (Gerfen & Surmeier, 2011; Graveland & DiFiglia, 1985). This conclusion raises questions about the identity of the other active neurons as several striatal interneurons are spontaneously active (Assous et al., 2018; Tepper & Koós, 2017). Some spontaneously active neurons may belong to different populations of interneurons.

On the other hand, besides their typical firing during whole-cell recordings, a variable uncorrelated firing rate, typical of in vivo recordings, was also found in vitro using

calcium imaging. Calcium imaging allowed us to record several PV+ neurons simultaneously over brief periods of time, including firing evoked by preserved excitatory inputs. This firing was uncorrelated either with other PV+ or PV− neurons' activity. The lack of significant correlated activity between pairs of PV+ neurons despite previous reports of correlated firing (Gittis et al., 2010; Russo et al., 2013; Tepper & Koós, 2017) can be explained by the variability in firing patterns which is likely shaped by synaptic inputs and modulation, the period of recording time and low temporal resolution of calcium imaging recordings. CDFs of cell activity were not significantly different between PV− and PV+ neurons, in agreement with in vivo observations (Berke, 2008, 2011; Sharott et al., 2012).

4.2 | Microcircuit modifications after optogenetic activation of PV+ neurons in vitro

Feed-forward inhibition of PV+ neurons upon striatal SPNs has been reported in vitro (Gittis et al., 2010; Koós & Tepper, 1999) and in vivo (Burguiére, Monteiro, Feng, & Graybiel, 2013; Lee et al., 2018; Owen et al., 2018). Accordingly, we tested the action of these neurons in the striatal microcircuit with optogenetic activation using ChR2. In these conditions, light activation generated action potentials firing in PV+ neurons which in turn inhibited the firing of individual SPNs (Gittis et al., 2010; Koós & Tepper, 1999; Owen et al., 2018). Surprisingly, by following the activity of dozens of neurons simultaneously, the final microcircuit action of PV+ neurons depended on context. When the circuit was nearly silent at rest, without stimulation, PV+ neuron action was to activate more neurons than those inhibited. This result had been predicted (Burke, Rotstein, & Alvarez, 2017; Humphries et al., 2009) as a mostly quiet striatal circuit may be in part the result of lateral and interneuron inhibition. Then, inhibition of inhibitory neurons upon a constant excitatory drive may facilitate some of them.

Previous work has shown strong cortical and thalamic connectivity to PV+ striatal neurons (Arias-García et al., 2018; Assous & Tepper, 2019; Choi et al., 2019; Lee et al., 2019; Melzer et al., 2017; Ramanathan et al., 2002), which are more responsive than SPNs (Gittis et al., 2010; Koós et al., 2004; Mallet et al., 2005; Planert et al., 2010; Tecuapetla et al., 2007). Also, connections between SPNs (Chuhma, Tanaka, Hen, & Rayport, 2011; Czubayko & Plenz, 2002; Tecuapetla et al., 2007; Tunstall, Oorschot, Kean, & Wickens, 2002) whose lateral inhibition (Burke et al., 2017; Dobbs et al., 2016; Guzmán et al., 2003) and their differential responses to afferent inputs, dopamine (DA) and acetylcholine (ACh) may also help to achieve this result (Assous & Tepper, 2019; Dobbs et al., 2016; Flores-Barrera, Vizcarra-Chacón, Bargas, Tapia, & Galarraga, 2011; Flores-Barrera, Vizcarra-Chacón, Tapia, Bargas, & Galarraga, 2010; Garas et al., 2016; García-Vilchis et al., 2019; Gittis et al., 2010; Guzmán et al., 2003; Taverna, Canciani, & Pennartz, 2007; Tecuapetla et al., 2007; Tecuapetla, Koós, Tepper, Kabbani, & Yeckel, 2009). Therefore, one parsimonious interpretation of this apparently paradoxical result is that in a mostly inhibitory microcircuit PV+ neuron actions disinhibit more neurons than those inhibited (Burke et al., 2017; Humphries et al., 2009). Accordingly, the action of PV+ neurons has been correlated with movement initiation, movement speed and attention (Gritton et al., 2019; Kim et al., 2016; Roberts et al., 2019), and because microcircuit activation can be seen after cortical activation in vitro (Aparicio-Juárez et al., 2019), the observations taken together suggest that PV+ neuron actions help to shape or amplify excitatory commands, suggesting an additional role to that of feed-forward inhibition.

On the contrary, when the network is active showing temporal sequences of neuronal ensembles, PV+ neuron stimulation inhibited and activated different sets of neurons. Perhaps as expected, due to the local spread of their axonal field (Straub et al., 2016; Tepper & Koós, 2017) more neurons are inhibited. Nevertheless, a non-negligible amount of neurons are activated or unaffected. Inhibition and disinhibition (activation) working together are expected to turn on and off neuronal ensembles in order to alternate their activity to form temporal sequences. This is commonly seen in Central Pattern Generators or CPGs, capable to form ensemble sequences (Grillner & El Manira, 2015). In this class of circuits, incoming afferents choose sets of interneurons that in turn generate neuronal ensembles (Bikoff et al., 2016). Similar phenomena have partially been reported for the striatum (Assous & Tepper, 2019; Berke, 2011; Garas et al., 2016; Gittis et al., 2010; Klug et al., 2018; Lee et al., 2018; Owen et al., 2018; Russo et al., 2013; Sheng et al., 2019; Straub et al., 2016).

In fact, by observing functional connections (Fröhlich, 2016) and using graph analysis we could observe that neuronal ensembles in the striatum can be reconfigured after PV+ neuron activation, suggesting that afferent selection of interneuron sets is one underlying mechanism explaining the dynamics of microcircuits: alternation between neuronal ensembles forming sequences (Carrillo-Reid et al., 2008, 2009; Pérez-Ortega et al., 2016). Repetition, training and synaptic plasticity would make some ensemble sequences more stable than others (Calabresi, Pisani, Mercuri, & Bernardi, 1996; Martiros, Burgess, & Graybiel, 2018; Sheng et al., 2019).

ACKNOWLEDGEMENTS

We thank Dagoberto Tapia and Yazmín Ramiro-Cortes for technical support; Ariadna Aparicio-Juárez, Claudia

Rivera-Cerecedo, Héctor Alfonso Malagón-Rivero and Xochitl Ayala for their help in animal care facility; and Ana María Escalante and Francisco Pérez Eugenio for fixing computational incidents. Mariana Duhne is a doctoral student from Programa de Doctorado en Ciencias Biomédicas, Universidad Nacional Autónoma de México (UNAM), and received fellowship 270245 from CONACYT, México. Data in this work are part of her doctoral dissertation.

CONFLICT OF INTEREST

The authors declare no conflict of interest.

AUTHOR CONTRIBUTIONS

M.D., E.L-G., A.L. and J. B. conceived and designed the research. M.D., E.L-G., M.P-O. and M.A-G performed experiments. M.D. analysed data. M.D., E.L-G and J.B interpreted results of experiments. M.D. and F.A-C drafted the manuscript. J.B. and E.G. edited and revised the manuscript. M.D., J. B. and E.G. approved the final version of the manuscript.

DATA AVAILABILITY STATEMENT

The data for this paper are mainly composed of videos. Due to storage requirements, the data are not available but can be made available upon request.

ORCID

Mariana Duhne https://orcid.org/0000-0001-9987-6704
Elvira Galarraga https://orcid.org/0000-0002-1769-1245
José Bargas https://orcid.org/0000-0002-8205-8163

REFERENCES

Aparicio-Juárez, A., Duhne, M., Lara-González, E., Ávila-Cascajares, F., Calderón, V., Galarraga, E., & Bargas, J. (2019). Cortical stimulation relieves parkinsonian pathological activity in vitro. *European Journal of Neuroscience*, *49*, 834–848.

Arias-García, M. A., Tapia, D., Laville, J. A., Calderón, V. M., Ramiro-Cortés, Y., Bargas, J., & Galarraga, E. (2018). Functional comparison of corticostriatal and thalamostriatal postsynaptic responses in striatal neurons of the mouse. *Brain Structure & Function*, *223*, 1229–1253.

Assous, M., Faust, T. W., Assini, R., Shah, F., Sidibe, Y., & Tepper, J. M. (2018). Identification and characterization of a novel spontaneously active Bursty GABAergic interneuron in the mouse striatum. *Journal of Neuroscience*, *38*, 5688–5699.

Assous, M., & Tepper, J. M. (2019). Cortical and thalamic inputs exert cell type-specific feedforward inhibition on striatal GABAergic interneurons. *Journal of Neuroscience Research*. *97*, 1491–1502. https://doi.org/10.1002/jnr.24444

Barroso-Flores, J., Herrera-Valdez, M. A., Lopez-Huerta, V. G., Galarraga, E., & Bargas, J. (2015). Diverse short-term dynamics of inhibitory synapses converging on striatal projection neurons: differential changes in a rodent model of Parkinson's disease. *Neural Plasticity*, *2015*, 573543. https://doi.org/10.1155/2015/573543

Beatty, J. A., Song, S. C., & Wilson, C. J. (2015). Cell-type-specific resonances shape the responses of striatal neurons to synaptic input. *Journal of Neurophysiology*, *113*, 688–700.

Berke, J. D. (2008). Uncoordinated firing rate changes of striatal fastspiking interneurons during behavioral task performance. *Journal of Neuroscience*, *28*, 10075–10080.

Berke, J. D. (2011). Functional properties of striatal fast-spiking interneurons. *Frontiers in Systems Neuroscience*, *5*, 45.

Bikoff, J. B., Gabitto, M. I., Rivard, A. F., Drobac, E., Machado, T. A., Miri, A., … Jessell, T. M. (2016). Spinal inhibitory interneuron diversity delineates variant motor microcircuits. *Cell*, *165*, 207–219. https://doi.org/10.1016/j.cell.2016.01.027

Bounova, G., & de Weck, O. (2012). Overview of metrics and their correlation patterns for multiple-metric topology analysis on heterogeneous graph ensembles. *Physical Review*, *85*, 016117.

Burguiére, E., Monteiro, P., Feng, G., & Graybiel, A. M. (2013). Optogenetic stimulation of lateral orbitofronto-striatal pathway suppresses compulsive behaviors. *Science*, *340*, 1243–1246.

Burke, D. A., Rotstein, H. G., & Alvarez, V. A. (2017). Striatal local circuitry: A new framework for lateral inhibition. *Neuron*, *96*, 267–284. https://doi.org/10.1016/j.neuron.2017.09.019

Buzsaki, G. (2010). Neural syntax: Cell assemblies, synapsembles, and readers. *Neuron*, *68*, 362–385. https://doi.org/10.1016/j.neuron.2010.09.023

Calabresi, P., Pisani, A., Mercuri, N. B., & Bernardi, G. (1996). The corticostriatal projection: From synaptic plasticity to dysfunctions of the basal ganglia. *Trends in Neurosciences*, *19*, 19–24.

Carrillo-Reid, L., Hernández-López, S., Tapia, D., Galarraga, E., & Bargas, J. (2011). Dopaminergic modulation of the striatal microcircuit: Receptor-specific configuration of cell assemblies. *Journal of Neuroscience*, *31*, 14972–14983.

Carrillo-Reid, L., Tecuapetla, F., Ibáñez-Sandoval, O., Hernández-Cruz, A., Galarraga, E., & Bargas, J. (2009). Activation of the cholinergic system endows compositional properties to striatal cell assemblies. *Journal of Neurophysiology*, *101*, 737–749.

Carrillo-Reid, L., Tecuapetla, F., Tapia, D., Hernández-Cruz, A., Galarraga, E., Drucker-Colin, R., & Bargas, J. (2008). Encoding network states by striatal cell assemblies. *Journal of Neurophysiology*, *99*, 1435–1450.

Chen, T.-W., Wardill, T. J., Sun, Y., Pulver, S. R., Renninger, S. L., Baohan, A., … Kim, D. S. (2014). Ultrasensitive fluorescent proteins for imaging neuronal activity. *Nature*, *499*, 295–300. https://doi.org/10.1038/nature12354

Choi, K., Holly, E. N., Davatolhagh, M. F., Beier, K. T., & Fuccillo, M. V. (2019). Integrated anatomical and physiological mapping of striatal afferent projections. *European Journal of Neuroscience*, *49*, 626–636.

Chuhma, N., Tanaka, K. F., Hen, R., & Rayport, S. (2011). Functional connectome of the striatal medium spiny neuron. *Journal of Neuroscience*, *31*, 1183–1192.

Committee for the Update of the Guide for the Care and Use of Laboratory Animals, Institute for Laboratory Animal Research, Division on Earth and Life Studies (2011). *Guide for the care and use of laboratory animals eighth edition*. Washington, D.C.: The National Academies Press. www.nap.edu

Czubayko, U., & Plenz, D. (2002). Fast synaptic transmission between striatal spiny projection neurons. *Proceedings of the National Academy of Sciences*, *99*, 15764–15769.

Dana, H., Mohar, B., Sun, Y., Narayan, S., Gordus, A., Hasseman, J. P., … Kim, D. S. (2016). Sensitive red protein calcium indicators

for imaging neural activity. *Elife*, *5*, e12727. https://doi.org/10.7554/eLife.12727

Dobbs, L. K., Kaplan, A. R., Lemos, J. C., Matsui, A., Rubinstein, M., & Alvarez, V. A. (2016). Dopamine regulation of lateral inhibition between striatal neurons gates the stimulant actions of cocaine. *Neuron*, *90*, 1100–1113. https://doi.org/10.1016/j.neuron.2016.04.031

Doig, N. M., Moss, J., & Bolam, J. P. (2010). Cortical and thalamic innervation of direct and indirect pathway medium-sized spiny neurons in mouse striatum. *Journal of Neuroscience*, *30*, 14610–14618.

Flores-Barrera, E., Vizcarra-Chacón, B. J., Bargas, J., Tapia, D., & Galarraga, E. (2011). Dopaminergic modulation of corticostriatal responses in medium spiny projection neurons from direct and indirect pathways. *Frontiers in Systems Neuroscience*, *5*, 15.

Flores-Barrera, E., Vizcarra-Chacón, B. J., Tapia, D., Bargas, J., & Galarraga, E. (2010). Different corticostriatal integration in spiny projection neurons from direct and indirect pathways. *Frontiers in Systems Neuroscience*, *4*, 15.

Fröhlich, F. (2016). *Network neuroscience*. London, UK: Academic Press-Elsevier.

Garas, F. N., Shah, R. S., Kormann, E., Doig, N. M., Vinciati, F., Nakamura, K. C., … Sharott, A. (2016). Secretagogin expression delineates functionally-specialized populations of striatal parvalbumin-containing interneurons. *Elife*, *26*, 5. https://doi.org/10.7554/eLife.16088

García-Vilchis, B., Suárez, P., Serrano-Reyes, M., Arias-García, M., Tapia, D., Duhne, M., … Galarraga, E. (2019). Differences in synaptic integration between direct and indirect striatal projection neurons: Role of CaV 3 channels. *Synapse (New York, N. Y.)*, *73*, e22079.

Gerfen, C. R., & Surmeier, D. J. (2011). Modulation of striatal projection systems by dopamine. *Annual Review of Neuroscience*, *34*, 441–466.

Gittis, A. H., Leventhal, D. K., Fensterheim, B. A., Pettibone, J. R., Berke, J. D., & Kreitzer, A. C. (2011). Selective inhibition of striatal fast-spiking interneurons causes dyskinesias. *Journal of Neuroscience*, *31*, 15727–15731.

Gittis, A. H., Nelson, A. B., Thwin, M. T., Palop, J. J., & Kreitzer, A. C. (2010). Distinct roles of GABAergic interneurons in the regulation of striatal output pathways. *Journal of Neuroscience*, *30*, 2223–2234.

Graveland, G. A., & Difiglia, M. (1985). The frequency and distribution of medium sized neurons with indented nuclei in the primate and rodent neostriatum. *Brain Research*, *327*, 307–311.

Grillner, S., & El Manira, A. (2015). The intrinsic operation of the networks that make us locomote. *Current Opinion in Neurobiology*, *31*, 244–249.

Gritton, H. J., Howe, W. M., Romano, M. F., DiFeliceantonio, A. G., Kramer, M. A., Saligrama, V., … Han, X. (2019). Unique contributions of parvalbumin and cholinergic interneurons in organizing striatal networks during movement. *Nature Neuroscience*, *22*, 586–597.

Guzman, J. N., Hernandez, A., Galarraga, E., Tapia, D., Laville, A., Vergara, R., … Bargas, J. (2003). Dopaminergic modulation of axon collaterals interconnecting spiny neurons of the rat striatum. *Journal of Neuroscience*, *23*, 8931–8940.

Higgs, M. H., & Wilson, C. J. (2019). Frequency-dependent entrainment of striatal fast-spiking interneurons. *Journal of Neurophysiology*, *122*, 1060–1072.

Hippenmeyer, S., Vrieseling, E., Sigrist, M., Portmann, T., Laengle, C., Ladle, D. R., & Arber, S. (2005). A developmental switch in the response of DRG neurons to ETS transcription factor signalling. *PloS Biology*, *3*, 0878–0890.

Humphries, M. D., Wood, R., & Gurney, K. (2009). Dopamine-modulated dynamic cell assemblies generated by the GABAergic striatal microcircuit. *Neural Network*, *22*, 1174–1188.

Ibañez-Sandoval, O., Tecuapetla, F., Unal, B., Shah, F., Koos, T., & Tepper, J. M. (2010). Electrophysiological and morphological characteristics and synaptic connectivity of tyrosine hydroxylase-expressing neurons in adult mouse striatum. *Journal of Neuroscience*, *30*, 6999–7016.

Jáidar, O., Carrillo-Reid, L., Hernández, A., Drucker-Colín, R., Bargas, J., & Hernández-Cruz, A. (2010). Dynamics of the Parkinsonian striatal microcircuit: Entrainment into a dominant network state. *Journal of Neuroscience*, *30*, 11326–11336. https://doi.org/10.1523/JNEUROSCI.1380-10.2010

Jáidar, O., Carrillo-Reid, L., Nakano, Y., Lopez-Huerta, V. G., Hernandez-Cruz, A., Bargas, J., … Arbuthnott, G. W. (2019). Synchronized activation of striatal direct and indirect pathways underlies the behavior in unilateral dopamine-depleted mice. *European Journal of Neuroscience*, *49*, 1512–1528.

Jin, X., Tecuapetla, F., & Costa, R. M. (2014). Basal ganglia subcircuits distinctively encode the parsing and concatenation of action sequences. *Nature Neuroscience*, *17*, 423–430.

Kawaguchi, Y., Wilson, C. J., Augood, S. J., & Emson, P. C. (1995). Striatal interneurons: Chemical, physiological and morphological characterization. *Trends in Neurosciences*, *18*, 527–535.

Kim, D., Jeong, H., Lee, J., Ghim, J. W., Her, E. S., Lee, S. H., & Jung, M. W. (2016). Distinct roles of parvalbumin- and somatostatin-expressing interneurons in working memory. *Neuron*, *92*, 902–915. https://doi.org/10.1016/j.neuron.2016.09.023

Kincaid, A. E., Zheng, T., & Wilson, C. J. (1998). Connectivity and convergence of single corticostriatal axons. *Journal of Neuroscience*, *18*, 47224731.

Kita, H., Kosaka, T., & Heizmann, C. W. (1990). Parvalbumin-immunoreactive neurons in the rat neostriatum: A light and electron microscopic study. *Brain Research*, *536*, 1–15. https://doi.org/10.1016/0006-8993(90)90002-S

Klaus, A., Martins, G. J., Paixao, V. B., Zhou, P., Paninski, L., & Costa, R. M. (2017). The spatiotemporal organization of the striatum encodes action space. *Neuron*, *95*, 1171–1180. https://doi.org/10.1016/j.neuron.2017.08.015

Klug, J. R., Engelhardt, M. D., Cadman, C. N., Li, H., Smith, J. B., Ayala, S., … Jin, X. (2018). Differential inputs to striatal cholinergic and parvalbumin interneurons imply functional distinctions. *Elife*, *7*, e35657.

Koós, T., & Tepper, J. M. (1999). Inhibitory control of neostriatal projection neurons by GABAergic interneurons. *Nature Neuroscience*, *2*, 467–472.

Koós, T., Tepper, J. M., & Wilson, C. J. (2004). Comparison of IPSCs evoked by spiny and fast-spiking neurons in the neostriatum. *Journal of Neuroscience*, *24*, 7916–7922.

Lara-González, E., Duhne, M., Ávila-Cascajares, F., Cruz, S., & Bargas, J. (2019). Comparison of actions between L-DOPA and different dopamine agonists in striatal DA-depleted microcircuits in vitro: Pre-clinical insights. *Neuroscience*, *410*, 76–96. https://doi.org/10.1016/j.neuroscience.2019.04.058

Lee, C. R., Yonk, A. J., Wiskerke, J., Paradiso, K. G., Tepper, J. M., & Margolis, D. J. (2019). Opposing influence of sensory and motor cortical input on striatal circuitry and choice behavior. *Current Biology*, *29*, 1313–1323.

Lee, K., Holley, S. M., Shobe, J. L., Chong, N. C., Cepeda, C., Levine, M. S., & Masmanidis, S. C. (2018). Parvalbumin interneurons modulate striatal output and enhance performance during associative learning. *Neuron*, *93*, 1451–2146. https://doi.org/10.1016/j.neuron.2017.02.033

López-Huerta, V. G., Carrillo-Reid, L., Galarraga, E., Tapia, D., Fiordelisio, T., Drucker-Colin, R., & Bargas, J. (2013). The balance of striatal feedback transmission is disrupted in a model of parkinsonism. *Journal of Neuroscience*, *33*, 4964–4975.

Luk, K. C., & Sadikot, A. F. (2001). GABA promotes survival but not proliferation of parvalbumin-immunoreactive interneurons in rodent neostriatum: An in vivo study with stereology. *Neuroscience*, *104*, 93–103. https://doi.org/10.1016/S0306-4522(01)00038-0

Madisen, L., Zwingman, T. A., Sunkin, S. M., Oh, S. W., Zariwala, H. A., Gu, H., … Zeng, H. (2010). A robust and high-throughput Cre reporting and characterization system for the whole mouse brain. *Nature Neuroscience*, *13*, 133–140.

Mallet, N., Le Moine, C., Charpier, S., & Gonon, F. (2005). Feedforward inhibition of projection neurons by fast-spiking GABA interneurons in the rat striatum in vivo. *Journal of Neuroscience*, *25*, 3857–3869.

Martiros, N., Burgess, A. A., & Graybiel, A. M. (2018). Inversely active striatal projection neurons and interneurons selectively delimit useful behavioral sequences. *Current Biology*, *28*, 560–573.

Melzer, S., Gil, M., Koser, D. E., Michael, M., Huang, K. W., & Monyer, H. (2017). Distinct corticostriatal GABAergic neurons modulate striatal output neurons and motor activity. *Cell Reports*, *19*, 1045–1055. https://doi.org/10.1016/j.celrep.2017.04.024

Newman, M. E. J. (2003). The structure and function of complex networks. *SIAM Review*, *45*, 167–256.

Oh, S. W., Harris, J. A., Ng, L., Winslow, B., Cain, N., Mihalas, S., … Zeng, H. (2014). A mesoscale connectome of the mouse brain. *Nature*, *508*, 207–214. https://doi.org/10.1038/nature13186

Owen, S. F., Berke, J. D., & Kreitzer, A. C. (2018). Fast-spiking interneurons supply feedforward control of bursting, calcium, and plasticity for efficient learning. *Cell*, *172*, 683–695.e15. https://doi.org/10.1016/j.cell.2018.01.005

Parthasarathy, H. B., & Graybiel, A. M. (1997). Cortically driven immediate-early gene expression reflects modular influence of sensorimotor cortex on identified striatal neurons in the squirrel monkey. *Journal of Neuroscience*, *17*, 2477–2491. https://doi.org/10.1523/JNEUROSCI.17-07-02477.1997

Pérez-Ortega, J., Duhne, M., Lara-González, E., Plata, V., Gasca, D., Galarraga, E., & Bargas, J. (2016). Pathophysiological signatures of functional connectomics in parkinsonian and dyskinetic striatal microcircuits. *Neurobiology of Diseases*, *91*, 347–361.

Planert, H., Szydlowski, S. N., Hjorth, J. J., Grillner, S., & Silberberg, G. (2010). Dynamics of synaptic transmission between fast-spiking interneurons and striatal projection neurons of the direct and indirect pathways. *Journal of Neuroscience*, *30*, 3499–3507.

Ramanathan, S., Hanley, J. J., Deniau, J. M., & Bolam, J. P. (2002). Synaptic convergence of motor and somatosensory cortical afferents onto GABAergic interneurons in the rat striatum. *Journal of Neuroscience*, *22*, 8158–8169. https://doi.org/10.1523/JNEUROSCI.22-18-08158.2002

Rehani, R., Atamna, Y., Tiroshi, L., Chiu, W. H., Aceves Buendía, J. J., Martins, G. J., … Goldberg, J. A. (2019). Activity patterns in the neuropil of striatal cholinergic interneurons in freely moving mice represent their collective spiking Dynamics. *eNeuro*, *6*, pii: ENEURO.0351-18.2018. https://doi.org/10.1523/ENEURO.0351-18.2018

Rendón-Ochoa, E. A., Laville, A., Tapia, D., Cáceres-Chávez, V. A., Hernández-Flores, T., Duhne, M., … Bargas, J. (2018). Calcium currents in striatal fast-spiking interneurons: Dopaminergic modulation of CaV1 channels. *BMC Neuroscience*, *19*, 1–14. https://doi.org/10.1186/s12868-018-0441-0

Roberts, B. M., White, M. G., Patton, M. H., Chen, R., & Mathur, B. N. (2019). Ensemble encoding of action speed by striatal fast-spiking interneurons. *Brain Structure & Function*, *224*, 2567–2576.

Russo, G., Nieus, T. R., Maggi, S., & Taverna, S. (2013). Dynamics of action potential firing in electrically connected striatal fast-spiking interneurons. *Frontiers in Cellular Neuroscience*, *7*, 209.

Rymar, V. V., Sasseville, R., Luk, K. C., & Sadikot, A. F. (2004). Neurogenesis and stereological morphometry of calretinin-immunoreactive GABAergic interneurons of the neostriatum. *The Journal of Comparative Neurology*, *469*, 325–339.

Sciamanna, G., & Wilson, C. J. (2011). The ionic mechanism of gamma resonance in rat striatal fast-spiking neurons. *Journal of Neurophysiology*, *106*, 2936–2949.

Sharott, A., Doig, N. M., Mallet, N., & Magill, P. J. (2012). Relationships between the firing of identified striatal interneurons and spontaneous and driven cortical activities in vivo. *Journal of Neuroscience*, *32*, 13221–13236.

Sheng, M.-J., Lu, D., Shena, Z.-M., & Poo, M.-M. (2019). Emergence of stable striatal D1R and D2R neuronal ensembles with distinct firing sequence during motor learning. *Proceedings of the National Academy of Sciences of the United States of America*, *16*, 11038–11047.

Straub, C., Saulnier, J. L., Begue, A., Feng, D. D., Huang, K. W., & Sabatini, B. L. (2016). Principles of synaptic organization of GABAergic interneurons in the striatum. *Neuron*, *92*, 84–92. https://doi.org/10.1016/j.neuron.2016.09.007

Surmeier, D. J., Carrillo-Reid, L., & Bargas, J. (2011). Dopaminergic modulation of striatal neurons, circuits, and assemblies. *Neuroscience*, *19*, 3–18.

Taverna, S., Canciani, B., & Pennartz, C. M. (2007). Membrane properties and synaptic connectivity of fast-spiking interneurons in rat ventral striatum. *Brain Research*, *1152*, 49–56.

Tecuapetla, F., Carrillo-Reid, L., Bargas, J., & Galarraga, E. (2007). Dopaminergic modulation of short-term synaptic plasticity at striatal inhibitory synapses. *Proceedings of the National Academy of Sciences of the United States of America*, *104*, 10258–10263.

Tecuapetla, F., Jin, X., Lima, S. Q., & Costa, R. M. (2016). Complementary contributions of striatal projection pathways to action initiation and execution. *Cell*, *166*, 703–715. https://doi.org/10.1016/j.cell.2016.06.032

Tecuapetla, F., Koós, T., Tepper, J. M., Kabbani, N., & Yeckel, M. F. (2009). Differential dopaminergic modulation of neostriatal synaptic connections of striatopallidal axon collaterals. *Journal of Neuroscience*, *29*, 8977–8990. https://doi.org/10.1523/JNEUROSCI.6145-08.2009

Tecuapetla, F., Matias, S., Dugue, G. P., Mainen, Z. F., & Costa, R. M. (2014). Balanced activity in basal ganglia projection pathways is critical for contraversive movements. *Nature Communications*, *5*, 4315.

Tepper, J. M., & Bolam, J. P. (2004). Functional diversity and specificity of neostriatal interneurons. *Current Opinion in Neurobiology*, *14*, 685692.

Tepper, J. M., & Koos, T. (2017). Striatal GABAergic interneurons. In H. Steiner, & K. Tseng (Eds.), *Handbook of Basal Ganglia Structure and Function 2nd Edition, Handbook of Behavioral Neuroscience*, Vol. *24* (pp. 157–178). Cambridge, MA: Academic Press.

Tepper, J. M., Tecuapetla, F., Koos, T., & Ibanñez-Sandoval, O. (2010). Heterogeneity and diversity of striatal GABAergic interneurons. *Frontiers in Neuroanatomy*, *4*, 150.

Tunstall, M. J., Oorschot, D. E., Kean, A., & Wickens, J. R. (2002). Inhibitory interactions between spiny projection neurons in the rat striatum. *Journal of Neurophysiology*, *88*, 1263–1269. https://doi.org/10.1152/jn.2002.88.3.1263

Wu, Y., Richard, S., & Parent, A. (2000). The organization of the striatal output system: A single-cell juxtacellular labeling study in the rat. *Neuroscience Research*, *38*, 49–62. https://doi.org/10.1016/S0168-0102(00)00140-1

Xu, M., Li, L., & Pittenger, C. (2016). Ablation of fast-spiking interneurons in the dorsal striatum, recapitulating abnormalities seen post-mortem in Tourette syndrome, produces anxiety and elevated grooming. *Journal of Neuroscience*, *324*, 321–329. https://doi.org/10.1016/j.neuroscience.2016.02.074

SUPPORTING INFORMATION

Additional supporting information may be found online in the Supporting Information section.

How to cite this article: Duhne M, Lara-González E, Laville A, et al. Activation of parvalbumin-expressing neurons reconfigures neuronal ensembles in murine striatal microcircuits. *Eur J Neurosci*. 2020;00:1–16. https://doi.org/10.1111/ejn.14670

Discusión

Actividad espontánea de neuronas PV+ *in vitro*

Previamente, hemos usado la imagenología de calcio para estudiar la actividad neuronal del microcircuito estriatal (Aparicio-Juárez *et al.*, 2019; Carrillo-Reid *et al.*, 2008; Pérez-Ortega *et al.*, 2016). Este trabajo se centró en los efectos de la activación de neuronas PV+ en la dinámica del microcircuito estriatal al identificar y estimular estas neuronas en animales transgénicos y activarlas con ChR2. Los registros electrofisiológicos (Figura 1c) muestran que la imagenología de calcio puede subestimar la actividad de neuronas PV+ que se encuentran disparando de manera tónica a alta frecuencia (Chen *et al.*, 2014; Roberts *et al.*, 2019). Sin embargo, este disparo rara vez se encuentra de manera espontánea (Sharott *et al.*, 2012) posiblemente por la interacción entre propiedades de membrana y entradas sinápticas (Higgs & Wilson, 2019). Otra fuente de subestimación en nuestro caso puede venir de la línea transgénica usada: PV-IRES-Cre. Se ha reportado que esta línea tiene una baja penetrancia genética en comparación con la línea PV-2A (Madisen *et al.*, 2010; Owen *et al.*, 2018). Sin embargo, aún con las limitantes expresadas, la participación de las neuronas PV+ en un circuito activo o estimulado fue del 5-11 % de las neuronas activas incluso si, anatómicamente, son menos del 1% de las neuronas en el circuito (Figura 2b, Luk & Sadikot, 2001). Concluimos que su actividad relativa en la red es mayor que la de neuronas PV-, en su mayoría SPNs (Gerfen & Surmeier 2011; Graveland & DiFiglia, 1985). Esta conclusión plantea dudas sobre la identidad de las otras neuronas activas ya que se ha reportado que otras interneuronas también tienen actividad espontánea (Assous & Tepper, 2018; Tepper & Koós, 2017). Es probable que algunas

de las neuronas tónicamente activas pertenezcan a diferentes poblaciones de interneuronas ya que muchas de ellas tienen disparo espontáneo o de tipo marcapaso (Tepper *et al.*, 2010).

Por otro lado, además del disparo a alta frecuencia en registros en la configuración de célula entera, *in vitro* con imagenología de calcio encontramos actividad variable y poco correlacionada (Figura 2d), similar a la comúnmente encontrada en registros *in vivo* (Berke, 2008; 2011). Esta técnica, nos permitió registrar la actividad de varias neuronas PV+ de manera simultánea en largos periodos de tiempo, incluyendo actividad provocada por entradas excitatorias preservadas. Esta actividad se encuentra de correlacionada con la actividad de otras neuronas PV+ o PV- (Figura 2d). La falta de actividad correlacionada significativamente entre pares de neuronas PV+ ha sido reportada previamente (Gittis *et al.*, 2010; Russo *et al.*, 2013; Tepper & Koós, 2017), puede deberse a la variabilidad en los patrones de actividad, que son moldeados por entradas sinápticas y moduladoras, el periodo de registro, así como a la baja resolución temporal de los registros de imagenología de calcio. Las CDFs de la actividad celular no mostró diferencias significativas entre neuronas PV+ y PV- (Figura 2c), lo que concuerda con observaciones *in vivo* (Sharott *et al.*, 2012).

Modificación de la actividad del microcircuito después de la estimulación optogenética de neuronas PV+ *in vitro*

Se ha reportado que las neuronas PV+ proveen inhibición *feedforward* a las SPNs *in vitro* (Gittis, *et al.*, 2010; Koós and Tepper, 1999) e *in vivo* (Burguiére *et al.*, 2013; Lee *et al.*, 2018; Owen *et al.*, 2018). Por ello, primero probamos la acción de estas neuronas en el microcircuito estriatal con activación optogenética, usando ChR2, en un tejido sin estimulación y con

actividad espontánea (Figura 4). En estas condicionas, la luz generó el disparo de potenciales de acción en las neuronas PV+, que a su vez inhibieron el disparo de potenciales de acción en las SPNs (Figura 3e, Gittis *et al.*, 2010; Koós & Tepper, 1999; Owen *et al.*, 2018). Inesperadamente, al seguir la actividad de docenas de neuronas simultáneamente, el efecto final de las neuronas PV+ en la actividad del circuito depende del contexto. Cuando el circuito se encontraba en reposo o sin estimulación, la activación de neuronas PV+ accionó más neuronas de las que inhibió (Figura 4a-b). Trabajos previos demostraron una fuerte conexión cortical y talámica hacia las neuronas PV+ estriatales (Arias-García *et al.*, 2018; Choi *et al.*, 2019; Lee *et al.*, 2019; Ramanathan *et al.*, 2002) las cuales son más responsivas que las SPNs (Mallet *et al.*, 2005). Si a esto sumamos la conexión lateral inhibidora entre las SPNs (Burke *et al.*, 2017; Chuhma *et al.*, 2011; Czubayko & Plenz, 2002; Dobbs *et al.*, 2016; Guzmán *et al.*, 2003; Tecuapetla *et al.*, 2007; Tunstall *et al.*, 2002) y su respuesta diferente ante entradas sinápticas o moduladoras de dopamina y acetilcolina, puede suceder que la activación de neuronas inhibidoras en un circuito inhibidor produzca desinhibición (Dobbs *et al.*, 2016; Flores-Barrera *et al.*, 2010; 2011; Gittis *et al.*, 2010; Guzmán *et al.*, 2003; Taverna *et al.*, 2007; Tecuapetla *et al.*, 2007; 2009). Lo cual lleva al resultado de que la acción de las neuronas PV+ es desinhibir (activar) más neuronas de las que inhibe (Figura 4e). Esto había sido predicho en trabajos de modelación (Burke *et al.*, 2017; Humphries *et al.*, 2009) ya que la baja actividad estriatal en un circuito en reposo es resultado de una fuerte inhibición lateral y de las interneuronas; la inhibición de una red inhibitoria puede llevar a la desinhibición. Esto concuerda con que la acción de las neuronas PV+ ha sido correlacionada con la iniciación del movimiento, su velocidad y la atención (Gritton *et al.*, 2019; Kim *et al.*, 2016; Roberts *et al.*, 2019). Como la activación del microcircuito se observa después

de una estimulación cortical *in vitro* (Aparicio-Juárez *et al.*, 2019), se puede sugerir que la acción de neuronas PV+ es ayudar a dar forma o amplificar los comandos corticales, sugiriendo que el papel de estas interneuronas no es solamente la inhibición *feedforward*.

En cambio, cuando la red ya se encuentra activa, mostrando secuencias temporales de activación de ensambles neuronales, la estimulación de neuronas PV+ deprimió y facilitó diferentes grupos de neuronas (Figura 5). Sin embargo, en este caso como era de esperarse (Straub *et al.*, 2016; Tepper & Koós, 2017) más neuronas fueron deprimidas. No obstante, una cantidad nada despreciable de neuronas se activaron o no fueron afectadas por la estimulación. La inhibición y la desinhibición (activación) parecen trabajar de manera conjunta para activar e inhibir ensambles neuronales, lo cual podría ser uno de los procesos que genere la alternancia entre ellos en forma de secuencias temporales. Esto se ha observado en patrones generadores de pautas o CPGs por sus siglas en inglés, capaces de formar secuencias de ensambles (Grillner & El Manira, 2015). En esta clase de circuitos, las aferentes eligen grupos de interneuronas que a su vez generan ensambles neuronales de manera temporal (Bikoff *et al.*, 2016). Fenómenos similares han sido parcialmente reportados en el estriado (Berke, 2011; Gittis *et al.*, 2010; Klug *et al.*, 2018; Lee *et al.*, 2018; Owen *et al.*, 2018; Russo *et al.*, 2013; Sheng *et al.*, 2019; Straub *et al.*, 2016).

Cuando observamos las conexiones funcionales entre las neuronas que forman los ensambles (Fröhlich, 2016) usando teoría de grafos, observamos que los ensambles neuronales son reconfigurados después de la activación de neuronas PV+ (Figura 6), sugiriendo que la preferencia de las aferentes por las interneuronas es un mecanismo que subyace a la dinámica de los microcircuitos: la alternancia de los ensambles formando secuencias (Carrillo-Reid *et al.*,

2008; 2009; Pérez-Ortega *et al.*, 2016). Repetición, entrenamiento y plasticidad sináptica harían algunas secuencias de ensambles más estables que otras (Calabresi *et al.*, 1996; Martiros *et al.*, 2018; Sheng *et al.*, 2019).

Conclusiones

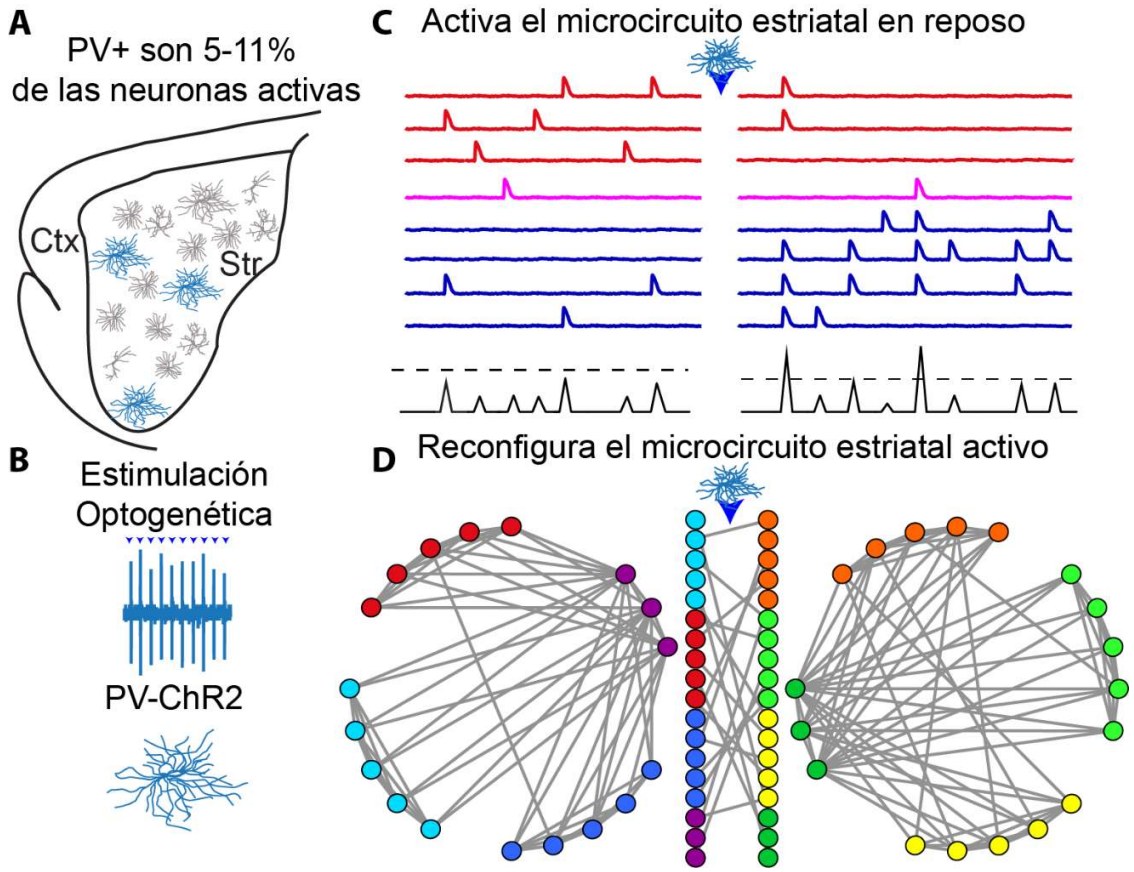

Figura 7 resumen gráfico. Representación esquemática de las conclusiones principales del trabajo. A. Las neuronas PV+ son del 5-11% de las neuronas activas en una rebanada registradas mediante imagenología de calcio. B. Se estimularon neuronas PV+ mediante optogenética. Esta estimulación inhibió el disparo de SPNs. C. La estimulación de neuronas PV+ en rebanadas en reposo provoca un incremento de actividad. D. La activación de neuronas PV+ en un circuito activo genera la reconfiguración de este.

Las interneuronas PV+ se encuentran participando de manera espontánea en el microcircuito estriatal activado. Son 5-10% de las neuronas activas monitoreadas con imagenología de calcio (Fig. 7A). Al activar a las neuronas PV+ con optogenética (Fig. 7B) en un microcircuito en reposo, el efecto dominante en la red es una activación que dura varios minutos.

Aunque hay neuronas que bajan su actividad en respuesta al estímulo (Fig. 7C). El mismo protocolo de estimulación en un microcircuito activo inhibe más neuronas que las que activa. Esto es, nuestros experimentos demuestran que las interneuronas inhibidoras clásicas *feedforward*, llamadas FSI y que expresan PV (canastas y candelabros), no sólo sirven para inhibir, simultáneamente desinhiben o activan diferentes grupos neuronales. Ambas acciones llevadas al cabo simultáneamente llevan a la reconfiguración de las conexiones funcionales de los ensambles neuronales, lo que puede ser un mecanismo para que el microcircuito genere las secuencias de ensambles neuronales (Fig. 7D).

Referencias

Aparicio-Juárez, A., Duhne, M., Lara-González, E., Ávila-Cascajares, F., Calderón, V., Galarraga, E. & Bargas, J. (2019) Cortical stimulation relieves parkinsonian pathological activity in vitro. *Eur. J. Neurosci.*, **49**, 834-848.

Arias-García, M.A., Tapia, D., Laville, J.A., Calderón, V.M., Ramiro-Cortés, Y., Bargas, J. & Galarraga, E. (2018) Functional comparison of corticostriatal and thalamostriatal postsynaptic responses in striatal neurons of the mouse. *Brain Struct. Funct.,* **223**, 1229-1253.

Assous, M., & Tepper, J.M. (2019) Cortical and thalamic inputs exert cell type-specific feedforward inhibition on striatal GABAergic interneurons. *J. Neuroci. Res., 97: 1491-1502*

Barnes TD, Kubota Y, Hu D, Jin DZ, Graybiel AM. (2005) Activity of striatal neurons reflects dynamic encoding and recoding of procedural memories. *Nature*, **437**, 1158-1161.

Beatty, J.A., Song, S.C. & Wilson, C.J. (2015) Cell-type-specific resonances shape the responses of striatal neurons to synaptic input. *J. Neurophysiol.*, **113**, 688-700.

Berke, J.D., (2008) Uncoordinated firing rate changes of striatal fastspiking interneurons during behavioral task performance. *J. Neurosci.*, **28**, 10075-10080.

Berke, J.D., (2011) Functional properties of striatal fast-spiking interneurons. *Front. Syst. Neurosci.*, **5**, 45.

Bikoff, J.B., Gabitto, M.I., Rivard, A.F., Drobac, E., Machado, T.A., Miri, A., Brenner-Morton, S., Famojure, E., Diaz, C., Alvarez, F.J., Mentis, G.Z. & Jessell, T.M. (2016) Spinal Inhibitory Interneuron Diversity Delineates Variant Motor Microcircuits. *Cell*, **165**, 207-219.

Bounova, G., & de Weck, O. (2012) Overview of metrics and their correlation patterns for multiple-metric topology analysis on heterogeneous graph ensembles*. Phys. Rev.*, **85**, 016117.

Brown, T. G. (1911) The intrinsic factors in the act of progression in the mammal. *Philos. Trans. R. Soc. Lond. B Biol. Sci.* **84**, 309–319.

Burguiére, E., Monteiro, P., Feng, G., Graybiel, A.M. (2013) Optogenetic stimulation of lateral orbitofronto-striatal pathway suppresses compulsive behaviors. Science., **340,** 1243-1246.

Burke, D. A., Rotstein, H. G., & Alvarez, V. A. (2017) Striatal Local Circuitry: A New Framework for Lateral Inhibition. *Neuron*, **96**, 267–284.

Buzsaki, G. (2010) Neural syntax: cell assemblies, synapsembles, and readers. *Neuron,* **68**, 362-385.

Calabresi, P., Pisani, A., Mercuri, N. B. & Bernardi, G. (1996) The corticostriatal projection: from synaptic plasticity to dysfunctions of the basal ganglia. *Trends Neurosci.*, **19**, 19–24.

Carrillo-Reid, L., Tecuapetla, F., Tapia, D., Hernández-Cruz, A., Galarraga, E., Drucker-Colin, R. & Bargas, J. (2008) Encoding network states by striatal cell assemblies. *J. Neurophysiol.*, **99**, 1435-50.

Carrillo-Reid, L., Tecuapetla, F., Ibáñez-Sandoval, O., Hernández-Cruz, A., Galarraga, E. & Bargas, J. (2009) Activation of the cholinergic system endows compositional properties to striatal cell assemblies. *J. Neurophysiol*., **101**, 737-49.

Chen, T.-W., Wardill, T. J., Sun, Y., Pulver, S. R., Renninger, S. L., Baohan, A., Schreiter, E.R., Kerr, R.A., Orger, M.B., Jayaraman, V., Looger, L.L., Svoboda, K. & Kim, D. S. (2014) Ultrasensitive fluorescent proteins for imaging neuronal activity. *Nature*, **499**, 295–300.

Choi, K., Holly, E. N., Davatolhagh, M. F., Beier, K. T. & Fuccillo, M. V. (2019) Integrated anatomical and physiological mapping of striatal afferent projections. *Eur. J. Neurosci.*, **49**, 626-636.

Chuhma, N., Tanaka, K.F., Hen, R., & Rayport, S. (2011) Functional connectome of the striatal medium spiny neuron. *J. Neurosci.*, 31, 1183–1192.

Czubayko, U., & Plenz, D. (2002) Fast synaptic transmission between striatal spiny projection neurons. *Proc. Natl. Acad. Sci.,* **99**, 15764–15769.

Dana, H., Mohar, B., Sun, Y., Narayan, S., Gordus, A., Hasseman, J.P., Tsegaye1, G., Holt, G.T., Hu, A., Walpita, D., Patel, R., Macklin, J.J., Bargmann, C.I., Ahrens, M.B., Schreiter, E.R., Jayaraman, V., Looger, L.L., Svoboda1, K. & Kim D.S. (2016) Sensitive red protein calcium indicators for imaging neural activity. *Elife,* **5**, e12727.

Dobbs, L.K., Kaplan, A.R., Lemos, J.C., Matsui, A., Rubinstein, M., & Alvarez, V.A. (2016) Dopamine regulation of lateral inhibition between striatal neurons gates the stimulant actions of cocaine. *Neuron*, **90**, 1100–1113.

Doig, N.M., Moss, J., & Bolam, J.P. (2010) Cortical and thalamic innervation of direct and indirect pathway medium-sized spiny neurons in mouse striatum. *J. Neurosci*., **30**, 14610–14618.

Feldman, J.L., Mitchell, G.S., Nattie, E.E. (2003) Breathing: rhythmicity, plasticity, chemosensitivity. *Annu. Rev. Neurosci.*, **26**, 239-66.

Flores-Barrera, E., Vizcarra-Chacón, B.J., Tapia, D., Bargas, J. & Galarraga, E. (2010) Different corticostriatal integration in spiny projection neurons from direct and indirect pathways. *Front. Syst. Neurosci*., **4**,15.

Flores-Barrera, E., Vizcarra-Chacón, B.J., Bargas, J., Tapia, D. & Galarraga, E. (2011) Dopaminergic modulation of corticostriatal responses in medium spiny projection neurons from direct and indirect pathways. *Front. Syst. Neurosci.,* **5**, 15.

Fröhlich, F. (2016) Network Neuroscience. Academic Press-Elsevier, London.

Gerfen, C.R. & Surmeier, D.J. (2011) Modulation of striatal projection systems by dopamine. Annu. Rev. Neurosci., **34**, 441–466.

Gittis, A.H., Nelson, A.B., Thwin, M.T., Palop, J.J. & Kreitzer, A.C., (2010) Distinct roles of GABAergic interneurons in the regulation of striatal output pathways. *J. Neurosci.*, **30**, 2223-2234.

Gittis, A.H., Leventhal, D.K., Fensterheim, B.A., Pettibone, J.R., Berke, J.D. & Kreitzer, A.C., (2011) Selective inhibition of striatal fast-spiking interneurons causes dyskinesias. *J. Neurosci.*, **31**, 15727-15731.

Graveland, G.A. & Difiglia, M. (1985) The frequency and distribution of medium sized neurons with indented nuclei in the primate and rodent neostriatum. *Brain Res.,* **327**, 307-311.

Graybiel, A.M. (1995a) Building action repertoires: memory and learning functions of the basal ganglia. *Curr. Opin. Neurobiol.*, **5**, 733-741.

Graybiel, A.M. (1995b) The Basal Ganglia. *Trends Neurosci.* **18**, 60-62.

Grillner, S., Markram, H., De Schutter, E., Silberberg, G., LeBeau, F.E. (2005) Microcircuits in action--from CPGs to neocortex. *Trends Neurosci.*, **28**, 525-533.

Grillner, S. & El Manira, A. (2015) The intrinsic operation of the networks that make us locomote. *Curr. Opin. Neurobiol.*, **31**, 244–249.

Gritton, H.J., Howe, W.M., Romano, M.F., DiFeliceantonio, A.G., Kramer, M.A., Saligrama, V., Bucklin, M.E., Zemel, D., Han, X. (2019) Unique contributions of parvalbumin and

cholinergic interneurons in organizing striatal networks during movement. *Nat. Neurosci.,* **22**, 586-597

Guzman, J.N., Hernandez, A., Galarraga, E., Tapia, D., Laville, A., Vergara, R., Aceves, J. & Bargas, J., (2003) Dopaminergic modulation of axon collaterals interconnecting spiny neurons of the rat striatum. *J. Neurosci.,* **23**, 8931-8940.

Hebb, D. O. (1949) *The Organization of Behavior.* Wiley, New York.

Higgs, M.H. & Wilson, C.J. (2019) Frequency-dependent entrainment of striatal fast-spiking interneurons. *J. Neurophysiol.*, **122**, 1060-1072.

Hippenmeyer, S., Vrieseling, E., Sigrist, M., Portmann, T., Laengle, C., Ladle, D. R., & Arber, S. (2005) A developmental switch in the response of DRG neurons to ETS transcription factor signalling. *PloS Biology*, **3**, 0878–0890.

Humphries, M.D., Wood, R. & Gurney, K. (2009) Dopamine-modulated dynamic cell assemblies generated by the GABAergic striatal microcircuit. *Neural Netw.*, **22**, 1174-1188.

Ibañez-Sandoval, O., Tecuapetla, F., Unal, B., Shah, F., Koos, T., Tepper, J.M. (2010) Electrophysiological and morphological characteristics and synaptic connectivity of tyrosine hydroxylase-expressing neurons in adult mouse striatum. *J. Neurosci.*, **30**:6999–7016.

Jáidar, O., Carrillo-Reid, L., Hernández, A., Drucker-Colín, R., Bargas, J. & Hernández-Cruz, A. (2010) Dynamics of the Parkinsonian striatal microcircuit: entrainment into a dominant network state. *J. Neurosci.*, **30**, 11326-11336.

Jin, X., Tecuapetla, F. & Costa, R.M. (2014) Basal ganglia subcircuits distinctively encode the parsing and concatenation of action sequences. *Nat. Neurosci*., **17**, 423–430.

Kawaguchi, Y. (1993). Physiological, morphological, and histochemical characterization of three classes of interneurons in rat neostriatum. *J. Neurosci.* **13**, 4908–4923.

Kawaguchi, Y., Wilson, C.J., Augood, S.J., Emson, P.C. (1995) Striatal interneurons: chemical, physiological and morphological characterization. Trends. *Neurosci.*, **18**:527–535.

Kim, D., Jeong, H, Lee, J., Ghim, J.W., Her, E.S., Lee, S.H. & Jung, M.W. (2016) Distinct Roles of Parvalbumin- and Somatostatin-Expressing Interneurons in Working Memory. *Neuron*, **92**, 902-915.

Kita, H., Kosaka, T. & Heizmann, C.W. (1990) Parvalbumin-immunoreactive neurons in the rat neostriatum: a light and electron microscopic study. *Brain Res.*, **536**, 1-15.

Klaus, A., Martins, G. J., Paixao, V. B., Zhou, P., Paninski, L., & Costa, R. M. (2017). The spatiotemporal organization of the striatum encodes action space. *Neuron*, **95**, 1171-1180.

Klug, J. R., Engelhardt, M. D., Cadman, C. N., Li, H., Smith, J. B., Ayala, S., Williams, E.W., Hoffman, H. & Jin, X. (2018). Differential inputs to striatal cholinergic and parvalbumin interneurons imply functional distinctions. *Elife*, **7**, e35657.

Koós, T. & Tepper, J.M. (1999) Inhibitory control of neostriatal projection neurons by GABAergic interneurons. *Nat. Neurosci.,* **2,** 467-72.

Koós, T., Tepper, J.M. & Wilson, C.J. (2004) Comparison of IPSCs evoked by spiny and fast-spiking neurons in the neostriatum. *J. Neurosci.*, **24**, 7916–7922.

Lara-González, E., Duhne, M., Ávila-Cascajares, F., Cruz, S. & Bargas, J. (2019) Comparison of Actions between L-DOPA and Different Dopamine Agonists in Striatal DA-Depleted Microcircuits In Vitro: Pre-Clinical Insights. *Neurosci.*, **410**, 76-96.

Lee, K., Holley, S. M., Shobe, J. L., Chong, N. C., Cepeda, C., Levine, M. S., & Masmanidis, S. C. (2018) Parvalbumin Interneurons Modulate Striatal Output and Enhance Performance during Associative Learning. *Neuron*, **93**, 1451–146.

Lee, C.R. , Yonk, A.J. , Wiskerke, J. , Paradiso, K.G. , Tepper, J.M. & Margolis, D.J. (2019) Opposing Influence of Sensory and Motor Cortical Input on Striatal Circuitry and Choice Behavior. *Curr. Biol.*, **29**, 1313–1323.

Luk,K.C. & Sadikot, A.F. (2001) GABA promotes survival but not proliferation of parvalbumin-immunoreactive interneurons in rodent neostriatum: an in vivo study with stereology. *Neurosci.*, **104**,93-103.

Madisen, L., Zwingman, T.A., Sunkin, S.M., Oh, S.W., Zariwala, H.A., Gu, H., Ng, L.L., Palmiter, R.D., Hawrylycz, M.J., Jones, A.R., Lein, E.S., Zeng, H. (2010) A robust and high-throughput Cre reporting and characterization system for the whole mouse brain. *Nat. Neurosci.*, **13**, 133-40.

Mallet, N., Le Moine, C., Charpier, S. & Gonon, F. (2005) Feedforward inhibition of projection neurons by fast-spiking GABA interneurons in the rat striatum in vivo. *J. Neurosci.*, **25**, 3857-3869.

Martiros, N., Burgess, A.A. & Graybiel, A.M. (2018) Inversely Active Striatal Projection Neurons and Interneurons Selectively Delimit Useful Behavioral Sequences. *Curr. Biol.*, **28**,560-573.

Muñoz-Manchado, A.B., Foldi, C., Szydlowski, S., Sjulson, L., Farries, M., Wilson, C., Silberberg, G., Hjerling-Leffler, J. (2016) Novel Striatal GABAergic Interneuron Populations Labeled in the 5HT3a(EGFP) Mouse. *Cereb. Cortex.*, **26** ,96-105.

Oh, S.W., Harris, J.A., Ng, L., Winslow, B., Cain, N., Mihalas, S., Wang, Q., Lau, C., Kuan, L., Henry, A.M., Mortrud, M.T., Ouellette, B., Nguyen, T.N., Sorensen, S.A., Slaughterbeck, C.R., Wakeman, W., Li, Y., Feng, D., Ho, A., Nicholas, E., Hirokawa, K.E., Bohn, P., Joines, K.M., Peng, H., Hawrylycz, M.J., Phillips, J.W., Hohmann, J.G., Wohnoutka, P., Gerfen, C.R., Koch, C., Bernard, A., Dang, C., Jones, A.R. & Zeng, H.(2014) A mesoscale connectome of the mouse brain. *Nature*, **508**, 207-14.

Ossowska, K., Wolfarth, S. (1995) Stimulation of glutamate receptors in the intermediate/caudal striatum induces contralateral turning. *Eur J Pharmacol.* **273**, 89-97.

Owen, S. F., Berke, J. D. & Kreitzer, A. C. (2018) Fast-Spiking Interneurons Supply Feedforward Control of Bursting, Calcium, and Plasticity for Efficient Learning. *Cell*, **172**, 683–695.e15.

Parthasarathy, H.B. & Graybiel, A.M. (1997) Cortically driven immediate-early gene expression reflects modular influence of sensorimotor cortex on identified striatal neurons in the squirrel monkey. *J. Neurosci.*, **17**, 2477-2491.

Pérez-Ortega, J., Duhne, M., Lara-González, E., Plata, V., Gasca, D., Galarraga, E. & Bargas, J. (2016) Pathophysiological signatures of functional connectomics in parkinsonian and dyskinetic striatal microcircuits. *Neurobiol. Dis.*, **91**, 347–361.

Planert, H., Szydlowski, S.N., Hjorth, J.J., Grillner, S. & Silberberg, G. (2010) Dynamics of synaptic transmission between fast-spiking interneurons and striatal projection neurons of the direct and indirect pathways. *J. Neurosci.*, **30**, 3499-3507.

Ramanathan, S., Hanley, J.J., Deniau, J.M. & Bolam, J.P. (2002) Synaptic convergence of motor and somatosensory cortical afferents onto GABAergic interneurons in the rat striatum. *J. Neurosci*, **22**, 8158-8169.

Rendón-Ochoa, E. A., Laville, A., Tapia, D., Cáceres-Chávez, V. A., Hernández-Flores, T., Duhne, M., Avilés-Rosas, V. H., Galarraga E. & Bargas J. (2018) Calcium currents in striatal fast-spiking interneurons: dopaminergic modulation of CaV1 channels. *BMC Neuroscience*, **19**, 1–14.

Roberts, B.M., White, M.G., Patton, M.H., Chen, R. & Mathur, B.N. (2019) Ensemble encoding of action speed by striatal fast-spiking interneurons. *Brain. Struc. Funct.*, **224**, 2567-2576.

Russo, G., Nieus, T.R., Maggi, S. & Taverna, S. (2013) Dynamics of action potential firing in electrically connected striatal fast-spiking interneurons. *Front. Cell. Neurosci.*, **7**, 209.

Rymar, V.V., Sasseville, R., Luk, K.C. & Sadikot, A.F., (2004) Neurogenesis and stereological morphometry of calretinin-immunoreactive GABAergic interneurons of the neostriatum. *J. Comp. Neurol.*, **469**, 325-339.

Selverston A. (1999) General principles of rhythmic motor pattern generation derived from invertebrate CPGs. *Prog. Brain Res.*, **123**, 247-57.

Sharott, A., Doig, N.M., Mallet, N. & Magill, P.J. (2012) Relationships between the firing of identified striatal interneurons and spontaneous and driven cortical activities in vivo. *J. Neurosci.*, **32**, 13221-13236.

Sheng, M-J., Lu, D., Shena, Z-M. & Poo, M-M. (2019) Emergence of stable striatal D1R and D2R neuronal ensembles with distinct firing sequence during motor learning. *Proc. Natl. Acad. Sci. U.S.A.*, **16**, 11038-11047.

Straub, C., Saulnier, J.L., Begue, A., Feng, D.D., Huang, K.W. & Sabatini, B.L. (2016) Principles of Synaptic Organization of GABAergic Interneurons in the Striatum. *Neuron*, **92**, 84–92.

Surmeier, D.J., Carrillo-Reid, L., Bargas, J. (2011) Dopaminergic modulation of striatal neurons, circuits, and assemblies. *Neurosci.*, **19**, 3–18.

Taverna, S., Canciani, B. & Pennartz, C.M. (2007) Membrane properties and synaptic connectivity of fast-spiking interneurons in rat ventral striatum. *Brain Res.*, **1152**, 49-56.

Tecuapetla, F., Carrillo-Reid, L., Bargas, J. & Galarraga, E. (2007) Dopaminergic modulation of short-term synaptic plasticity at striatal inhibitory synapses. *Proc. Natl. Acad. Sci. U.S.A.*, **104**, 10258-10263.

Tecuapetla, F., Koós, T., Tepper, J.M., Kabbani, N. & Yeckel, M.F. (2009). Differential dopaminergic modulation of neostriatal synaptic connections of striatopallidal axon collaterals. *J. Neurosci.*, **29**, 8977-8990.

Tecuapetla, F., Matias, S., Dugue, G.P., Mainen, Z.F. & Costa, R.M. (2014) Balanced activity in basal ganglia projection pathways is critical for contraversive movements. *Nat. Commun.,* **5**, 4315.

Tecuapetla, F., Jin, X., Lima, S. Q., & Costa, R. M. (2016) Complementary contributions of striatal projection pathways to action initiation and execution. *Cell*, **166**, 703–715.

Tepper, J.M. & Bolam, J.P. (2004) Functional diversity and specificity of neostriatal interneurons. *Curr. Opin. Neurobiol.*, **14**, 685692.

Tepper, J.M., Tecuapetla, F., Koos, T., Ibanñez-Sandoval, O. (2010) Heterogeneity and diversity of striatal GABAergic interneurons. *Front. Neuroanat.*, **4** 150.

Tepper, J.M. & Koos, T. (2017) Striatal GABAergic interneurons. In Steiner, H. & Tseng, K. (Eds), *Handbook of Basal Ganglia Structure and Function* 2nd Edition, *Handbook of Behavioral Neuroscience*, **24**, Academic Press, Cambridge, MA, 157–178.

Tunstall, M.J., Oorschot, D.E., Kean, A. & Wickens, J.R. (2002). Inhibitory interactions between spiny projection neurons in the rat striatum. *J. Neurophysiol*. **88**, 1263–1269.

Turner, R. S., and Desmurget, M. (2010). Basal ganglia contributions to motor control: a vigorous tutor. *Curr. Opin. Neurobiol.* **20**, 704–716.

Vergara, R., Rick, C., Hernández-López, S., Laville, J.A., Guzman, J.N., Galarraga, E., Surmeier, D.J., Bargas, J. (2003). Spontaneous voltaje oscillations in striatal projection neurons in a rat corticostriatal slice. *J Physiol*. **553**, 169-82.

Xu, M., Li, L. & Pittenger, C. (2016) Ablation of fast-spiking interneurons in the dorsal striatum, recapitulating abnormalities seen post-mortem in Tourette syndrome, produces anxiety and elevated grooming. *J. Neurosci.*, **324**, 321-329.

Yeung, M. Y., Ding, Q., Brooks, C. R., Xiao, S., Workman, C. J., Vignali, D. A. A. & Florida, C. C. (2016) A mesoscale connectome of the mouse brain. *Nature*, **15**, 942–95.